


Review

Next-Generation Molecular Imaging of Thyroid Cancer

Yuchen Jin ^{1,2,3,†}, Beibei Liu ^{4,†}, Muhsin H. Younis ⁵, Gang Huang ¹, Jianjun Liu ¹, Weibo Cai ^{5,6,*} 
and Weijun Wei ^{1,*}

¹ Department of Nuclear Medicine, Renji Hospital, School of Medicine, Shanghai Jiao Tong University, 1630 Dongfang Rd., Shanghai 200127, China; yuchenjin@sjtu.edu.cn (Y.J.); huang2802@163.com (G.H.); nuclearj@163.com (J.L.)

² Department of Nuclear Medicine, Shanghai Sixth People's Hospital Affiliated to Shanghai Jiao Tong University, Shanghai 200233, China

³ Human Oncology and Pathogenesis Program, Memorial Sloan-Kettering Cancer Center, New York, NY 10065, USA

⁴ Institute of Diagnostic and Interventional Radiology, Shanghai Sixth People's Hospital Affiliated to Shanghai Jiao Tong University, Shanghai 200233, China; beibei4906@163.com

⁵ Departments of Radiology and Medical Physics, University of Wisconsin–Madison, Madison, WI 53705-2275, USA; muhsinhy@gmail.com

⁶ Carbone Cancer Center, University of Wisconsin, Madison, WI 53705, USA

* Correspondence: wcai@uwhealth.org (W.C.); weijun.wei@outlook.com (W.W.); Tel.: +86-160-8262-1749 (W.C.)

† Yuchen Jin and Beibei Liu contributed equally to this work.

Simple Summary: Molecular imaging utilizes radionuclides or artificially modified molecules to image particular targets or pathways which are important in the pathogenesis of a certain disease. Transporter-based probes like radioiodine and [¹⁸F]fluoro-D-glucose ([¹⁸F]FDG) are widely used for diagnosing thyroid cancer (TC) and predicting the prognosis thereafter. However, newly developed probes (peptide, antibody, nanoparticle probes, and aptamer) image the fine molecular changes involved in the pathogenesis of TC and enable target-specific diagnosis and treatment of TC. Furthermore, novel molecular probes have high specificity and sensitivity, imparting a high level of objectivity to the research areas of TC.

Abstract: An essential aspect of thyroid cancer (TC) management is personalized and precision medicine. Functional imaging of TC with radioiodine and [¹⁸F]FDG has been frequently used in disease evaluation for several decades now. Recently, advances in molecular imaging have led to the development of novel tracers based on aptamer, peptide, antibody, nanobody, antibody fragment, and nanoparticle platforms. The emerging targets—including HER2, CD54, SHP2, CD33, and more—are promising targets for clinical translation soon. The significance of these tracers may be realized by outlining the way they support the management of TC. The provided examples focus on where preclinical investigations can be translated. Furthermore, advances in the molecular imaging of TC may inspire the development of novel therapeutic or theranostic tracers. In this review, we summarize TC-targeting probes which include transporter-based and immuno-based imaging moieties. We summarize the most recent evidence in this field and outline how these emerging strategies may potentially optimize clinical practice.

Keywords: thyroid cancer; molecular imaging; theranostics; companion diagnostics; immunoPET



Citation: Jin, Y.; Liu, B.; Younis, M.H.; Huang, G.; Liu, J.; Cai, W.; Wei, W. Next-Generation Molecular Imaging of Thyroid Cancer. *Cancers* **2021**, *13*, 3188. <https://doi.org/10.3390/cancers13133188>

Academic Editors: Fabio Medas and Pier Francesco Alesina

Received: 4 May 2021
Accepted: 22 June 2021
Published: 25 June 2021

Publisher's Note: MDPI stays neutral with regard to jurisdictional claims in published maps and institutional affiliations.



Copyright: © 2021 by the authors. Licensee MDPI, Basel, Switzerland. This article is an open access article distributed under the terms and conditions of the Creative Commons Attribution (CC BY) license (<https://creativecommons.org/licenses/by/4.0/>).

1. Introduction

Thyroid cancer (TC) is one of the most common cancer types and its occurrence has been rapidly increasing over the last several years [1]. TC represents around 2–2.3% of new cancer cases and 0.2–0.4% of deaths from all cancer types [2,3]. In 2021, the USA may have approximately 44,280 new cases of TC and about 2200 deaths [2]. Around 90,000 new cases along with 6800 deaths were estimated in 2015 in China [2]. By 2030, TC is anticipated

to become the second-most common type of cancer in females and the ninth in males [3]. 90–95% of cases present either papillary TC (PTC) or follicular TC (FTC), both of which originate from follicular cells in the thyroid and can be referred to as differentiated TC (DTC) [1].

In DTC, the thyroid retains the ability to absorb and store nearly all of the iodine in the whole body, providing the rationale for combined therapeutics with thyroidectomy and ^{131}I (a beta-emitting radioisotope of iodine) therapy [4]. A total or near-total thyroidectomy removes all or most of the thyroid and DTC tissue, facilitating DTC control and the subsequent ^{131}I ablation, adjuvant therapy, or therapy for DTCs [5]. The ^{131}I tends to concentrate in remnant thyroid tissue, latent DTC foci, and metastatic DTC lesions. The radiation can damage the remnant thyroid tissue and DTC cells, helping DTC re-staging and improving DTC prognosis [5,6]. Unfortunately, within 10 years of an initial thyroidectomy, local recurrence and distant metastases take place in approximately 10–20% of DTCs. Notwithstanding ^{131}I management, only one-third of DTCs could be regarded as having shown “complete response” with the remaining DTCs refractory to ^{131}I (i.e., radioiodine refractory DTC, RR-DTC) having a poor prognosis [7].

Two less common types of TC are medullary TC (MTC) and anaplastic TC (ATC), accounting for <5% of all TC cases. Notably, however, 50–80% of MTCs show widespread metastasis at the initial diagnosis, with a five-year survival rate of 38% [8]. Furthermore, ATC is tremendously aggressive with its median overall survival of less than one year [8,9]. Thus, it is necessary to find latent lesions, precisely evaluate the grade of malignancy, adopt the most effective therapeutics, and take precautions against local recurrence or distant metastasis on time.

Traditional diagnosis methods include thyroid physical exams, blood tests (for testing biomarkers such as thyroglobulin and calcitonin), ultrasound imaging (for helping determine whether a thyroid nodule or lymph node is likely to be benign or cancerous), and other imaging tests such as CT and MRI (for TC staging and determining TC spread) [5]. In recent decades, molecular imaging (MI) has become an increasingly popular approach, applying radionuclides or artificially modified molecules to assist clinicians in locating biomarkers, potential therapeutic targets, or describing signaling pathways [10,11]. These targets play a vital role in the diagnosis and management of TC, allowing for characterization and quantification of the molecular composition of tumor tissues [12]. MI has been shown to improve diagnosis of TC, personalized management, and long-term predictive prognosis index [13]. Moreover, MI is crucial to actualizing multimodality-based theranostic strategies for TCs [14].

Over the past decade, significant progress has been made in the application of MI to TC. For instance, nanobodies and aptamers have been used to elucidate the bio-features of TC. These tracers show an antigen-binding ability resembling that of traditional antibodies [15–18]. Furthermore, immuno-single photon emission computerized tomography (immunoSPECT) and immuno-positron emission tomography (immunoPET) have encouraged the development of new theranostic methods intended for complex clinical settings, particularly for the RR-DTCs or ATCs [19]. These methods provide opportunities for obtaining deep insights into the pathogenesis of TC and as well as novel therapeutic targets for TC. Indeed, the discovery and translation of new probes enabling precise theranostics of TC are urgently needed, especially for RR-DTCs and ATCs.

Primary references are mainly derived from PubMed (available before 7 June 2021), comprehensively including the pivotal evidence in the field. In this review, transporter-based platforms are updated, and newer tracers like aptamer-, peptide-, antibody-, nanobody-, and nanoparticle-based platforms for TC are summarized. We highlight some of the potentially translatable probes in the current review. We also outline how these emerging strategies may potentially improve clinical practice.

2. Transporter-Targeting Probes

Most transporter-targeting probes are small-size molecules, carried into the intracellular space by transporters on the cell surface. Some transporter-associated probes may take part in cell metabolism [20,21]. Many transporter-based isotopes, including radioiodine, are routinely to image the recurrence and metastases of TC. Several alternatives to radioiodine can identify RR-DTC metastases lacking radioiodine uptake. Other transporter-based radiotracers like [^{201}Tl]TlCl, [$^{99\text{m}}\text{Tc}$]Tc-sestamibi ([$^{99\text{m}}\text{Tc}$]Tc-MIBI), [$^{99\text{m}}\text{Tc}$]Tc-tetrofosmin, [$^{99\text{m}}\text{Tc}$]Tc-depreotide, [^{111}In]In-diethylenetriaminepentaacetic acid-octreotide ([^{111}In]In-DTPA-octreotide), and [^{18}F]fluoro-D-glucose ([^{18}F]FDG) have been synthesized, tested, and validated as beneficial for diagnosing TC [5,22]. In particular, [^{18}F]FDG has been widely applied in the management of TC [5].

2.1. Sodium Iodine Symporter (NIS)-Targeting Probes

NIS is the protein mainly locating at the cell plasma membrane, which carries Na^+/I^- ions from the extracellular matrix into the intracellular fluid [23]. The transported iodine, as an element, helps produce thyroid hormone (iodide organification) [24]. Unlike the expression pattern of other tumor targets (low expression in normal tissues and high expression in tumor tissues), NIS is usually present at high levels in normal thyroid tissues and DTC cells, enabling radioiodine collection in normal thyroid and TC cells [25]. Nevertheless, NIS downregulation happens in RR-DTCs, poorly differentiated TCs (PDTCs), and ATCs, causing these TC cells hard to benefit much from radioiodine treatment [26].

2.1.1. Radioiodine

Radioiodine, a widely used radioisotope, has a crucial role in the diagnosis and treatment of DTC. There are several medically useful radioisotopes of iodine (^{125}I , ^{131}I , and ^{124}I , etc.). However, only ^{131}I and ^{124}I are commonly applied in clinical settings due to their clinically acceptable radiation half-life, diagnostic or therapeutic performance, economic cost, and safety [27]. [^{131}I]NaI can track thyroid and TC cells with γ radiation on SPECT, and damage those cells by emitting β^- radiation [28]. [^{131}I]NaI allows ablation of thyroid remnant, adjuvant therapy of TC, and therapy of TC, which vastly improves the prognosis of patients with TC [5]. ^{124}I is another isotope of iodine emitting positron, which can be exploited for PET imaging. [^{124}I]NaI-PET/CT has superior spatial resolution and quantification ability over [^{131}I]NaI-SPECT [29].

Recently, numerous reports have focused on radioiodine for improving the diagnosis performance, and efficacy of treatment [30–32]. Tg tests coupled with iodine uptake assay [32], or [^{124}I]NaI PET/CT only [30,31], are used for ^{131}I dosimetry. Apart from performing dosimetry before ^{131}I treatment, much attention should be given to increase the membranous expression of NIS, induce the concentration of ^{131}I , and improve the therapeutic efficacy of ^{131}I treatment. For RR-DTC, PDTC, and ATC, it is essential to explore agents that could increase NIS expression and augment the migration of NIS to the cell membrane. These agents mainly include but are not limited to, retinoic acid [33], mechanistic target of rapamycin kinase (mTOR) inhibitors [34], and very recently, V-Raf murine sarcoma viral oncogene homolog B (BRAF) and mitogen-activated protein kinase kinase (MAP2K1/2, MEK1/2) inhibitors, which inhibit the extracellular signal-regulated kinase (ERK) pathway responsible for tumor progression and radioiodine uptake [35,36] (Figure 1). RR-DTCs would be stabilized, or shrinkage after treatment with kinase inhibitors, owing to the suppressed signaling pathway and enhanced ^{131}I treatment efficacy [26,37].

Lately, estrogen-related receptor gamma ($\text{ERR}\gamma$), one of the estrogen-related receptors, has gained more traction as a potential target to enhance or enable radioiodine uptake. $\text{ERR}\gamma$, a member of NR3B nuclear receptor superfamily, is a biomarker for multiple cancers, including breast cancer and prostate cancer [38]. Previous reports have shown that the $\text{ERR}\gamma$ inverse agonist GSK5182 increased NIS expression and NIS-mediated iodine uptake in Kirsten rat sarcoma viral oncogene homolog (KRAS) or BRAF mutated ATC cells in vitro [39]. In addition, another $\text{ERR}\gamma$ inverse agonist, DN200434, was recently shown to

increase the uptake of radioiodine in ATC tumors, identifying ERR γ as a target to enhance ^{131}I therapy responsiveness [40] (Figure 2). It remains to be determined if DN200434 has a re-differentiative effect in patients with either RR-DTC or ATC.

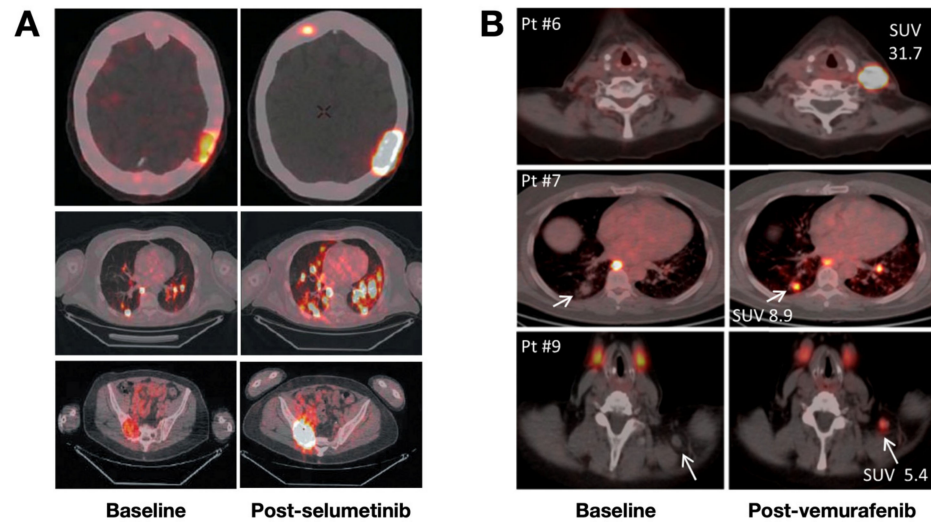


Figure 1. [^{124}I]NaI PET/CT images of patients with RR-DTC or PDTC with or without kinase inhibitors. (A) PET/CT images showed enhanced iodine uptake of lesions post-treatment with selumetinib in nearly all previously negative head, lung, and sacroiliac bone metastases. Reproduced with permission from [35], copyright 2013 Massachusetts Medical Society. (B) PET/CT images showed enhanced radioiodine uptake of lesions in the neck and lung after treatment with vemurafenib, a specific BRAF $^{\text{V600E}}$ inhibitor. Reproduced with permission from [36], copyright 2019 Endocrine Society.

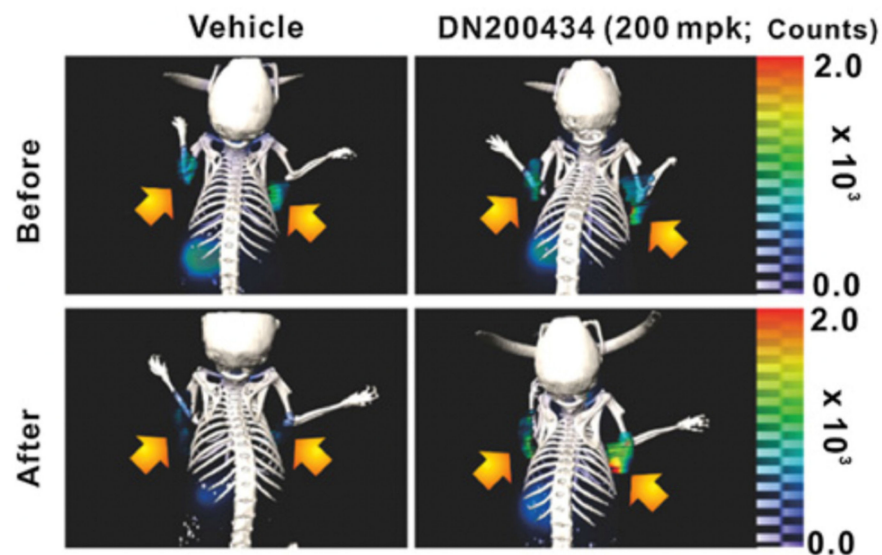


Figure 2. [^{124}I]NaI-PET/CT demonstrates enhanced iodine uptake in CAL62 ATC tumor after treatment with DN200434. The arrows indicate the ATC tumor. Reproduced with permission from [40], copyright 2019 American Association for Cancer Research.

2.1.2. [^{18}F]Tetrafluoroborate ([^{18}F]TFB)

Detecting local recurrence and metastases of DTC in radioiodine imaging is particularly important for the arrangement of local treatments, e.g., surgery or radiotherapy [5]. Whereas negative radioiodine imaging with increased serum thyroglobulin is a barrier for finding malignant lesions, the so-called “Thyroglobulin Elevated and Negative Iodine

Scintigraphy” (TENIS) needs radically diverse diagnostic and therapeutic methods [26]. TENIS could be caused by poor NIS expression, iodide organification defect, or radioiodine stunning [41,42]. A failure to find NIS-expressing DTC lesions might delay the diagnosis and also the timely onset of the treatment [43]. Despite [^{18}F]FDG-PET/CT could be applied for finding TENIS metastases, but its uptake might be partially caused by tumor-infiltrating immune cells [44]. Recently, [^{18}F]TFB, [^{18}F]Fluorosulfate ([^{18}F]FS), and [^{18}F]hexafluorophosphate ([^{18}F]HFP) have been discovered for imaging DTCs [45–48].

[^{18}F]TFB is an analog to radioiodine, having similar NIS affinities, same charge, and similar ionic radius to iodide. Therefore, [^{18}F]TFB can be transported by NIS [46,49] differed from radioiodine, [^{18}F]TFB can be readily synthesized at medical cyclotrons, and it provides a satisfactory half-life, dosing, biodistribution, and PET imaging quality [46,47] (Figure 3). [^{18}F]TFB-PET can exclusively reveal NIS expression in tumor cells, therefore reclassifying TENIS metastases into partial or complete dedifferentiation, and helping metastasis localization and prognosis evaluation [47]. [^{18}F]FS and [^{18}F]HFP are two other newly discovered NIS-targeting tracers having favorable targeting efficiency, image contrasts, and biodistribution features [45,48]. Although it has been reported that FS and HFP had higher NIS affinity than TFB [45], it remains unclear if [^{18}F]HFP and [^{18}F]FS are superior to [^{18}F]TFB. The clinical evaluation of the [^{18}F]HFP and [^{18}F]FS are still needed.

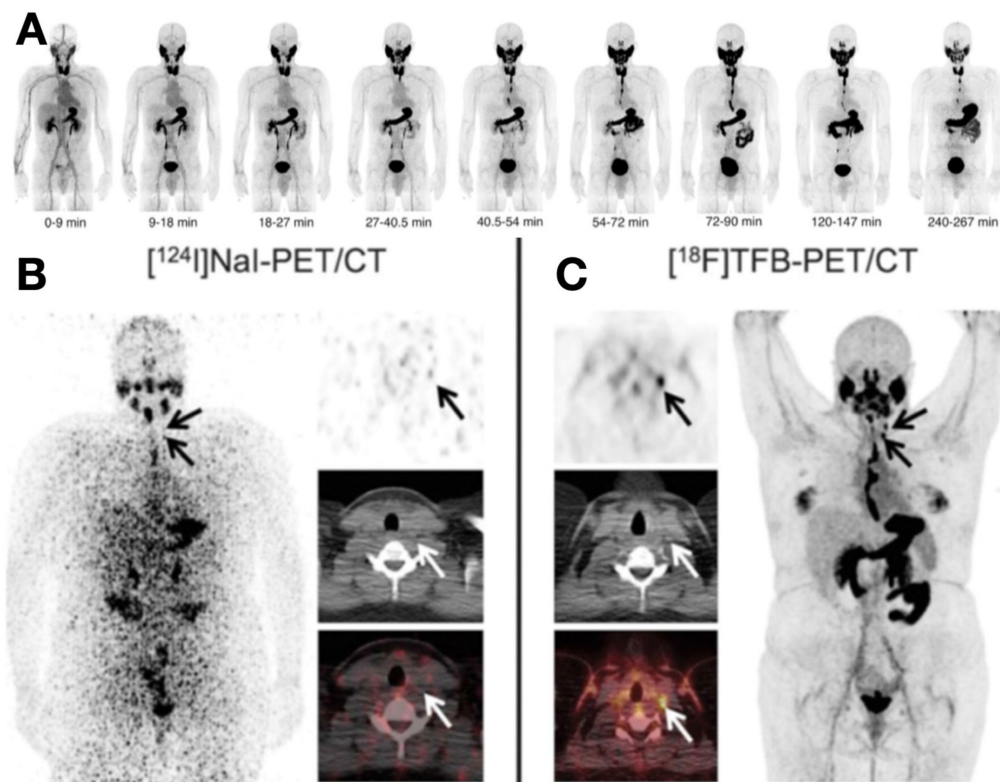


Figure 3. Evaluation of thyroid cancer via [^{18}F]TFB-PET/CT and [^{124}I]NaI-PET/CT. (A) Biodistribution of [^{18}F]TFB at various time points on PET images. [^{18}F]TFB accumulated rapidly in the thyroid and other normal tissues like the salivary gland and stomach within 10–30 min. Reproduced with permission from [50], copyright 2017 Society of Nuclear Medicine and Molecular Imaging. (B,C) A comparison between [^{124}I]NaI-PET/CT and [^{18}F]TFB-PET/CT in a 26-year-old patient post-thyroidectomy. (B) [^{124}I]NaI-PET/CT was unremarkable for PTC. (C) In contrast, [^{18}F]TFB-PET/CT revealed two foci in the left lateral cervical region. Reproduced with permission from [51], copyright 2018 Wolters Kluwer Health.

2.2. Glucose Transporter-Targeting Probes

[^{18}F]FDG, mainly transported by glucose-transporter family-1 (GLUT1), is a well-known radiopharmaceutical glucose analog used in clinical PET imaging [52]. Aggressive TCs with low radioiodine uptake generally show high levels of [^{18}F]FDG uptake [53].

[¹⁸F]FDG-PET/CT has shown great sensitivity in patients who otherwise do not benefit from ¹³¹I treatment. This is because metastases without radioiodine uptake tend to have high glycolytic rates, causing enhanced [¹⁸F]FDG uptake [54]. Furthermore, [¹⁸F]FDG can help detect TC recurrence or metastases and predict radioiodine uptake [54,55]. More specifically, [¹⁸F]FDG maximum standard unit value (SUV_{max}) higher than 4.0 would predict poor radioiodine uptake [54]. Besides, most PDTC, ATC, and MTC cells do not concentrate ¹³¹I. Thus, in these entities, [¹⁸F]FDG PET/CT imaging is useful in initial diagnosis, subsequent disease grading, treatment, and follow-up after treatment. Even though numerous glucose analog tracers other than [¹⁸F]FDG were created [56], their head-to-head comparisons with the widely used [¹⁸F]FDG are lacking.

2.3. Amino Acid Transporter-Targeting Probes

Alternatives to [¹⁸F]FDG are a subject of interest. Occasionally, [¹⁸F]FDG may yield inexplicable images. The false-positive [¹⁸F]FDG uptake happens in Hashimoto's disease and Graves' disease. In addition, it is hard to find brain metastasis on [¹⁸F]FDG PET/CT images because of the intense background signals [57,58]. In recent years, amino acid probes have obtained incremental attraction as alternatives to [¹⁸F]FDG. Amino acids probes include [¹⁸F]fluoro- α -methyl tyrosine ([¹⁸F]FAMT), [¹⁸F]fluoro-dihydroxyphenylalanine ([¹⁸F]FDOPA), L-[methyl-¹¹C]-methionine ([¹¹C]MET), [¹⁸F]fluoroethyl-tyrosine ([¹⁸F]FET), [¹⁸F]fluoroglutamine ([¹⁸F]FGln), and the newly discovered [¹⁸F]NKO-035. Of these, [¹⁸F]FDOPA, [¹¹C]MET, and [¹⁸F]FGln have been investigated in TCs [59–63].

2.3.1. [¹⁸F]FDOPA

[¹⁸F]FDOPA is a large neutral amino acid that resembles natural L-dopa, which can be transported by L-type amino acid transporter 1 (LAT1, SLC7A5) and L-type amino acid transporter 2 (LAT2, SLC7A8) [64]. [¹⁸F]FDOPA is a satisfactory probe for detecting MTC metastasis, persistence, and residual disease [59]. However, if [¹⁸F]FDOPA imaging is negative or unavailable, [¹⁸F]FDG should be considered, especially for aggressive MTCs displaying signs of dedifferentiation or rising carcinoma embryonic antigen (CEA) concentration in serum [59,65].

2.3.2. [¹¹C]MET

[¹¹C]MET, transported mainly by SLC7A5, is often used to visualize parathyroid adenoma and enable focused parathyroidectomy [66–68]. Published data for [¹¹C]MET in TC is limited. Only one case with hyperparathyroidism has been reported, which showed intense focal [¹¹C]MET uptake in a cold nodule with highly increased sestamibi uptake. The nodule was finally diagnosed as FTC, indicating the incremental value of [¹¹C]MET in imaging DTCs [63]. [¹¹C]MET is currently being studied as a surrogate for [¹⁸F]FDG in other tumor types, such as brain tumors [69,70] and laryngeal cancer [71]. To date, there is no evidence showing the superiority of [¹¹C]MET over [¹⁸F]FDG. Although complementary uptake of ¹¹C-MET and [¹⁸F]FDG has been reported in recurrent or metastatic DTCs [72], further clarification and longitudinal study are still required to illustrate the actual value of the [¹¹C]MET in clinic settings. The downside of [¹¹C]MET is the short half-life of ¹¹C (20.4 min), which limits its broad application [73].

2.3.3. [¹⁸F]FGln

[¹⁸F]FGln, an analog of natural glutamine regulated by several glutamine (Gln) transporters (solute carrier family 1 member 5, SLC1A5; solute carrier family 38 member 1, SLC38A1; and SLC7A5; etc.), has been tested and subsequently considered as a promising probe for assessing glutamine metabolism in tumors [61]. Its use is justified by the understanding that tumor cells need extra nutrition and energy for rapid growth and proliferation, while glutamine metabolism is occasionally used by the cell as an alternative to glucose [74]. [¹⁸F]FGln can further complement the diagnostic capacity of [¹⁸F]FDG by detecting Gln metabolic changes in PTCs [62]. In [¹⁸F]FGln imaging, excellent contrast

images can be made only 10 min after injection, while late-phase imaging (60 min) would cause a high background to some extent [62] (Figure 4).

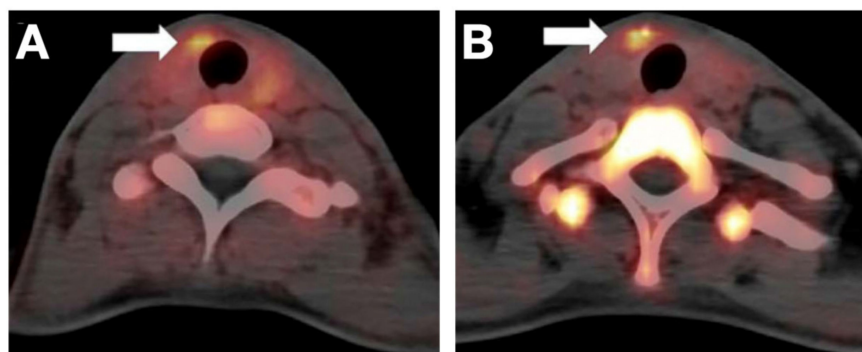


Figure 4. Example of a PTC revealed by [^{18}F]FGln at 10 min (A) and 60 min (B) post-injection, respectively. The arrows indicate the malignant lesion. Reproduced with permission from [62], copyright 2020 Springer Nature Inc.

[^{18}F]FAMT, [^{18}F]FET, and the newly reported [^{18}F]NKO-035 are all transported by L-type amino acid transporters, which are overexpressed in tumor cells [21,75]. However, data for those probes remain inadequate now. Furthermore, unlike other amino acid tracers transported by multiple unspecific amino acid transporters, [^{18}F]FAMT has an α -methyl moiety that allows it to be exclusively specific to SLC7A5, making it highly tumor-specific [76,77]. Furthermore, [^{18}F]FAMT is more specific for tumors than [^{18}F]FDG, although their sensitivities are similar. However, [^{18}F]FAMT imaging is comparable to [^{18}F]FDG imaging in diagnosing tumors other than TCs [20]. Future studies are warranted to investigate the amino acid metabolism in TCs and the diagnostic value of amino acid tracers in large cohorts.

2.4. Nucleoside Transporter-Targeting Probes

Radiolabeled or fluorescent nucleobase analogs are currently used to diagnose solid tumors, including cancers of the bladder, breast, lung, ovary, and pancreas. Regarding diagnosis of TC specifically, only [^{18}F]fluorothymidine ([^{18}F]FLT) has been tested to date. [^{18}F]FLT, which can be taken up by equilibrative nucleoside transporter 1 (ENT1), is a marker of cell proliferation [78]. In one study, 20 DTCs were assessed with [^{18}F]FLT and [^{18}F]FDG on PET/CT. While 69% of the metastatic lesions were identified by focal increases in [^{18}F]FLT uptake, a lower result than the 92% identified by [^{18}F]FDG PET/CT. It is also demonstrated that [^{18}F]FDG has the advantage in terms of specificity and accuracy over [^{18}F]FLT in finding local lymph node malignancy and distant metastases [79]. So far, [^{18}F]FLT PET/CT has not progressed very far in diagnosing TCs.

3. Peptide-Based Probes

Peptide tracers have played vital roles in MI due to their unique advantages, notably their low molecular weight and ability to bind tumor biomarkers specifically, with low toxicity to surrounding non-cancer cells. Multiple tracers, like [^{68}Ga]Ga-dodecane tetraacetic acid labeled RGD2 ([^{68}Ga]Ga-DOTA-RGD2; RGD: Arg-Gly-Asp), [^{68}Ga]Ga-prostate specific membrane antigen ligand ([^{68}Ga]Ga-PSMA) with conjugates of N,N'-bis[2-hydroxy-5-(carboxyethyl)benzyl]ethylene diamine-N,N'-diacetic acid (HBED-CC) or DOTA, [^{68}Ga]Ga-DOTA-DGlu-Ala-Tyr-Gly-Trp-(N-Me)Nle-Asp-1-Nal-NH₂ ([^{68}Ga]Ga-DOTA-MGS5), [^{111}In]In-DTPA-octreotide, and other somatostatin analogs have been developed for imaging TCs, particularly MTCs and RR-DTCs [80].

3.1. Somatostatin Receptor (SSTR)-Targeting Probes

Somatostatin receptors have become typical therapeutic targets in neuroendocrine tumors (NETs) because they are often overexpressed on the surface of tumor cells. This

has led to the development of several ^{68}Ga -labelled somatostatin analogs as PET imaging probes [81], which could be used for the diagnosis of MTC [80]. ^{68}Ga -labeled somatostatin analogs, including [^{68}Ga]Ga-DOTA-(1-Nal³)-octreotide ([^{68}Ga]Ga-DOTANOC), [^{68}Ga]Ga-DOTA(0)-Phe(1)-Tyr(3)-octreotide ([^{68}Ga]Ga-DOTATOC), and [^{68}Ga]Ga-DOTA-(Tyr3)-octreotate ([^{68}Ga]Ga-DOTATATE), are valuable diagnostic tools showing excellent performance in the majority of patients with NETs [82]. Nevertheless, studies reporting the diagnostic value of SSTR-targeted PET in recurrent MTC are limited. A meta-analysis involving nine studies reported that the tumor detection rate on SSTR-based PET or PET/CT is only 63.5% in recurrent MTC, which is lower than that in other NETs [83].

3.2. $\alpha\nu\beta 3$ Integrin-Targeting Probes

The integrin $\alpha\nu\beta 3$ expression on epithelial cells and mature endothelial cells is relatively low, however, it is commonly and highly expressed in solid tumors. RGD and RGD₂ are peptides that bind integrin $\alpha\nu\beta 3$ [84]. Recently, the dimeric [^{68}Ga]Ga-DOTA-RGD₂ has been successfully applied for PET imaging of RR-DTCs in clinical settings [85], showing sensitivity, specificity, and accuracy of 82.3%, 100%, and 86.4%, respectively, which exceeds the same measurements in [^{18}F]FDG of 82.3%, 50%, and 75%, respectively. For RR-DTCs, the advantage provided by [^{68}Ga]Ga-DOTA-RGD₂ is the ability to detect lesions not detected by [^{18}F]FDG [85] (Figure 5). Furthermore, diagnosis of RR-DTCs using [^{68}Ga]Ga-DOTA-RGD₂ is better accompanied by [^{177}Lu]Lu-DOTA-RGD₂, a potential treatment option for RR-DTCs [86]. Considering that [^{68}Ga]Ga-DOTA-RGD₂ and [^{177}Lu]Lu-DOTA-RGD₂ are a useful theranostic pair for RR-DTCs, the potential to improve the theranostic landscape of RR-DTCs by sequentially using these agents is high. Nuclear medicine approaches have revolutionized the theranostic arsenal for DTCs, and we are confident that there is room to optimize the management of RR-DTCs with these novel agents.

3.3. PSMA-Targeting Probes

PSMA is overexpressed on the prostate cancer cell membrane. Recently, several studies found unexpected PSMA-targeted radiotracer uptake by TCs, including RR-DTCs [87–91] (Figure 6). In addition, ~50% of TC microvessels showed high expression of PSMA related to tumor size and vascular invasion [89]. Thus, it is reasonable that high-grade TCs can be targeted by PSMA-specific radioligands like [^{177}Lu]Lu-PSMA and [^{225}Ac]Ac-PSMA [92], establishing a novel theranostic platform for TCs that are refractory to radioiodine treatment. Currently, the clinical interest and focus of PSMA-targeted theranostics remain primarily oriented towards prostate cancers. It is worth exploring the performance of PSMA-targeted agents in RR-DTCs. The authors wonder if PSMA-targeted agents will open a new horizon for RR-DTCs in the future.

3.4. Cholecystokinin-2 Receptor (CCK2R)-Targeting Probes

CCK2R is highly expressed in 90% of MTC, 50% of small cell lung cancers, 60% of astrocytomas, insulinomas, stromal ovarian cancers, gastrointestinal stromal tumors, and more than 20% of gastroenteropancreatic tumors [93–95]. As a new peptide tracer targeting CCK2R, ^{68}Ga -DOTA-MGS5 is supposed to be superior to [^{18}F]FDOPA in diagnosing MTCs. The comparison between the [^{68}Ga]Ga-DOTA-MGS5 and [^{18}F]FDOPA was performed in a 75-year-old female patient with recurrent MTC (calcitonin: 2726 ng/l), who underwent consecutive [^{68}Ga]Ga-DOTA-MGS5 and [^{18}F]FDOPA-PET/CT. [^{68}Ga]Ga-DOTA-MGS5 found three obvious liver lesions with higher uptake than [^{18}F]FDOPA-PET/CT (SUVmax = 6.4–8.3 vs. 3.7) and showed a good lesion-to-background contrast in the liver, which might yield complementary information to [^{18}F]FDOPA-PET in patients with recurrent MTC [96] (Figure 7). The background of [^{68}Ga]Ga-DOTA-MGS5 seems higher than that of [^{18}F]FDOPA in our opinion.

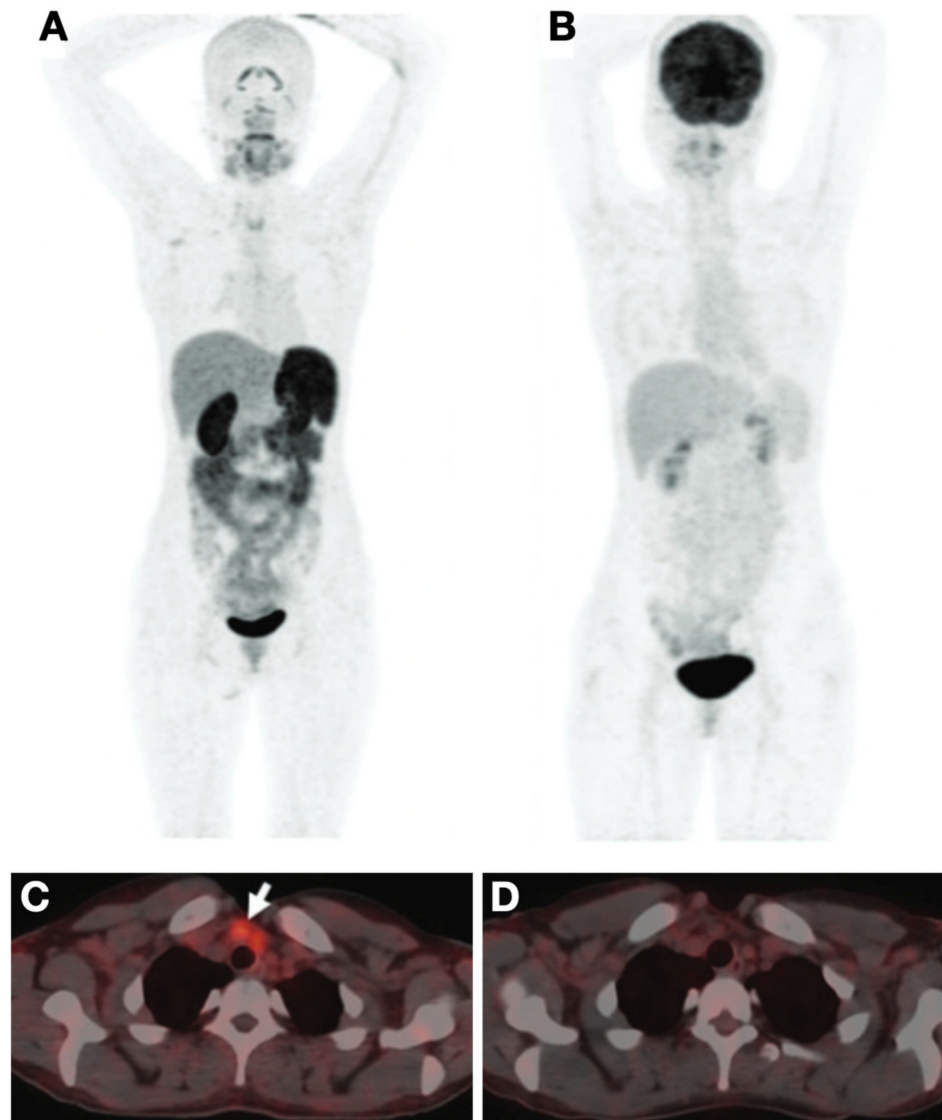


Figure 5. PET/CT imaging comparing $[^{68}\text{Ga}]\text{Ga-DOTA-RGD2}$ and $[^{18}\text{F}]\text{FDG}$. The RR-DTC case showed a high level of stimulated Tg (85 ng/mL) and negative ^{131}I post-therapy whole-body scan. Histopathology confirmed the metastatic lesions. (A) A maximum intensity projection (MIP) image showed $[^{68}\text{Ga}]\text{Ga-DOTA-RGD2}$ positive foci in the lower cervical region. (B) The corresponding MIP image of $[^{18}\text{F}]\text{FDG}$. (C) Fused PET/CT showed the metastatic foci was $[^{68}\text{Ga}]\text{Ga-DOTA-RGD2}$ positive; (D) the corresponding foci is negative on $[^{18}\text{F}]\text{FDG}$ fused PET/CT. Reproduced with permission from [85], copyright 2020 Mary Ann Liebert Inc.

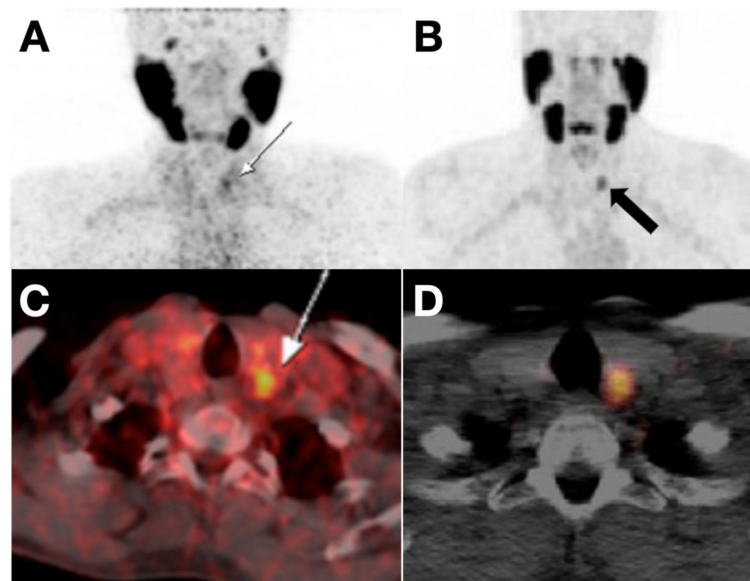


Figure 6. (A,C) PET and PET/CT fusion images showed slight [^{68}Ga]Ga-PSMA uptake in the thyroid nodule of a 62-year-old patient with prostate cancer. The thyroid nodule was validated as Hürthle cell angioinvasive FTC by post-thyroidectomy pathology. Reproduced with permission from [88] copyright 2016 Society of Nuclear Medicine and Molecular Imaging. (B,D) PET and PET/CT fusion image marked ^{68}Ga -PSMA uptake in the thyroid nodule of a 65-year-old man with metastatic prostate cancer. The thyroid nodule was regarded as TC proved by post-thyroidectomy pathology. Reproduced with permission from [91], copyright 2017 Wolters Kluwer Health Inc.

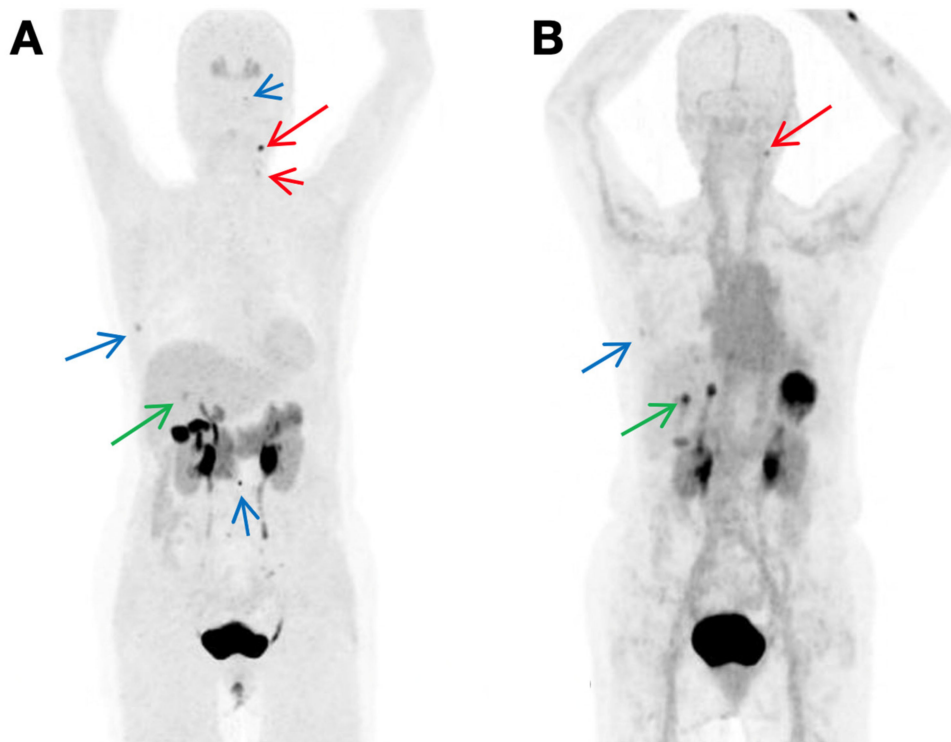


Figure 7. Comparison of [^{18}F]FDOPA and [^{68}Ga]Ga-DOTA-MGS5 in MTC patients. (A) [^{18}F]FDOPA PET imaging at one hour post-injection. (B) ^{68}Ga -Ga-DOTA-MGS5 PET imaging at one-hour post-injection. [^{68}Ga]Ga-DOTA-MGS5 yields complementary information to [^{18}F]FDOPA-PET. Reproduced with permission from [96], copyright 2021, Springer Nature Inc.

4. Antibody-Based Probes

Antibodies are high-affinity molecules with strict targeting abilities that are used for highly specific binding [97]. The development and translational use of antibody therapeutics have shaped the model of molecular targeted therapy and immunotherapy. The high affinity of monoclonal antibodies for their targets promotes the rational and efficacious use of antibody therapeutics [98]. We have advocated that PET imaging with radiolabeled antibodies or antibody fragments (i.e., immunoPET) provides a powerful platform for visualizing the tumor targets, selecting suitable patients for targeted therapies or immunotherapies, and assessing the therapeutic responses thereafter [19]. The first-generation monoclonal antibodies (mAbs) were of murine origin, making them immunogenic, limited for their clinical use. Consequently, chimeric mAbs, humanized mAbs, and complete human mAbs were produced to solve this issue [98]. One limitation of the full-size antibody probes is their considerable size (~150 kDa), which leads to a long circulatory half-life and reduced tissue penetration [99]. To ameliorate the imaging quality and efficiency and accelerate clinical translation, some smaller molecule substitute probes have been investigated, including antigen-binding fragments (Fabs) and engineered Fab variants, single-chain variable fragments (scFv), diabodies, minibodies (~25–100 kDa), and other types of therapeutic proteins, such as affibodies and nanobodies [19]. Facilitated by these developments, multiple antibodies, and antibody derivatives have been designed as either imaging probes or therapeutic agents to induce cancer cell death and elicit host immune effector responses in TC [19].

4.1. Single Target Immunoglobulin G (IgG) Probes

Full-size IgG antibody probes have been applied to tumor detection, staging, guidance of local treatment, identification or validation of tumor targets, and assessment of therapeutic response or tumor prognosis [100]. Once the first-rank antigen has been selected, the corresponding IgG can be labeled with a radionuclide or fluorescent tag [19]. The radionuclide labeled IgG can be visualized via immunoPET imaging, and the fluorescent tags can be visualized through the fluorescence system during thyroidectomy or metastasectomy [101].

4.1.1. Epidermal Growth Factor Receptor (HER2, ERBB2)-Targeting Probes

The human HER2, which is expressed on the cell plasma membrane [102], is a typical molecular marker for breast cancers and a subset of aggressive thyroid cancers [103,104]. HER2 overexpression was found in 44% of FTCs, 18% of PTCs [105], and certain ATCs [106]. Several HER2-specific agents—such as trastuzumab, lapatinib, and pertuzumab—have primarily ameliorated the prognosis in HER2-positive breast cancers [107,108]. Outside of breast cancers and TCs, HER2 is also widely overexpressed in multiple malignancies, including bladder, pancreatic, ovarian, and stomach cancers [109–111]. CUDC-101 (an inhibitor of epidermal growth factor receptor (EGFR), HER2, and histone deacetylase (HDAC)) inhibited tumor growth and metastases in metastatic ATC models [112], and lapatinib (an inhibitor of HER2 and EGFR) overcame the ERK and v-akt murine thymoma viral oncogene homolog 1 (AKT) rebound in PLX4032 resistant TC cells [113]. These studies indicate that HER2 is a potential target for developing theranostic interventions for advanced TCs.

By labeling the HER2-targeting mAb pertuzumab with ^{89}Zr , we have developed the [^{89}Zr]Zr-DFO-pertuzumab and evaluated its diagnostic efficacy in subcutaneous and orthotopic ATC models [114] (Figure 8). ImmunoPET and fluorescence imaging indicated that radiolabeled or fluorescence-labeled HER2 probes are promising for the management of ATCs, which may become helpful tools for image-guided tumor removal or identifying HER2-positive ATCs for HER2-targeted therapies. However, clinical studies are needed for further translation. To facilitate clinical translation and broad clinical use, we have developed a series of novel nanobody-based tracers to delineate HER2 expression. We will test the performance of the tracers in TC models very soon.

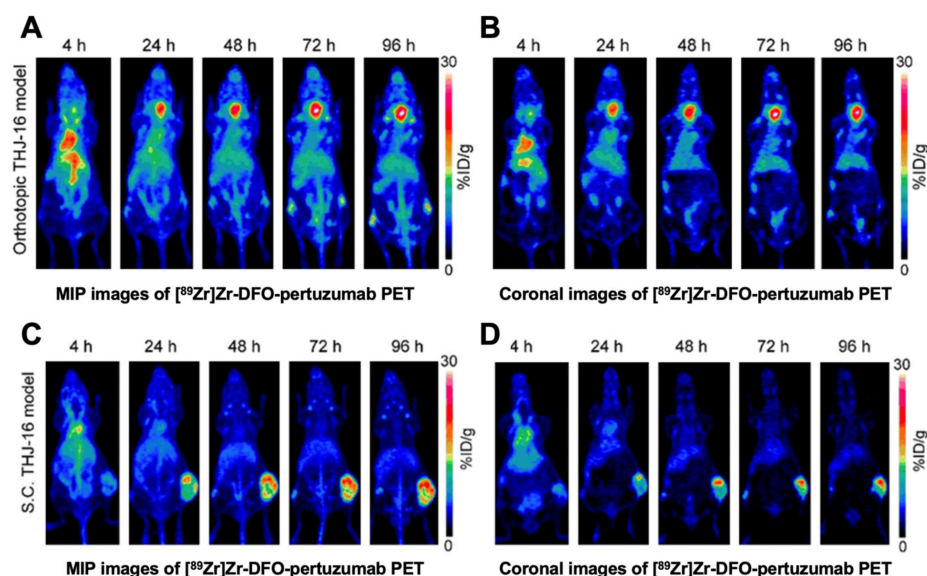


Figure 8. PET imaging with [^{89}Zr]Zr-DFO-pertuzumab in xenografts (cell line: THJ-16T). (A) Maximum intensity projection (MIP) showed the ability of [^{89}Zr]Zr-DFO-pertuzumab for visualizing TCs in an orthotopic model. (B) Coronal imaging in an orthotopic model. (C) MIP in a subcutaneous model. (D) Coronal imaging in a subcutaneous model. Reproduced with permission from [114], copyright 2019 e-Century Publishing Corporation.

4.1.2. Intercellular Adhesion Molecule-1 (ICAM-1, CD54)-Targeting Probes

ICAM-1, belonging to the immunoglobulin superfamily of cell adhesion molecules, consists of five extracellular IgG-like domains and one cytoplasmic tail [115]. ICAM-1 is found to be expressed at low levels in normal tissue, but at high levels in multiple types of cancer, including TCs [116,117]. One of its important features is that it can initiate tumor transmigration and invasion [116,118]. Furthermore, ICAM-1-targeted chimeric antigen receptor T (CAR-T) cells can robustly kill TC cells [119,120]. Research thus far has suggested ICAM-1 as an ideal target for TC diagnosis and treatments. For this purpose, Wei et al. created an immunoPET probe [^{64}Cu]Cu-NOTA-ICAM-1, which targets ICAM-1. [^{64}Cu]Cu-NOTA-ICAM-1 immunoPET imaging showed high contrast in diagnosing the subcutaneous and orthotopic ATCs in preclinical settings [101] (Figure 9). With the published data and unpublished data in hand, we believe that ICAM-1 may serve as a viable biomarker for certain types of TCs. However, it remains to see the diagnostic utility of ICAM-1-targeted tracers in patients with TCs.

4.1.3. Lectin Galactoside-Binding Soluble 3 (LGALS3, Galectin-3, or Gal3)-Targeting Probes

Gal-3 is a protein that is undetectable in normal and benign thyroid tissues but highly expressed in DTC cytosol, cell membranes, and intercellular substance [121]. The expression of galectin-3 as a biomarker for TCs has been validated in two multicenter studies [122,123]. The sensitivity and specificity of Gal-3 immunodetection reached 94% and 98% in distinguishing benign from TC lesions, with positive and negative predictive values of 98% and 94%, respectively, and diagnostic accuracy of 96% [122]. [^{89}Zr]Zr-labeled Gal3 mAb ([^{89}Zr]Zr-DFO-Gal3) or Gal-3 mAb with F(ab')₂ conjugation ([^{89}Zr]Zr-Gal3-F(ab')₂) has shown good binding to TC in vivo, allowing it to be potentially used for the detection of recurrence and metastases [124,125] (Figure 10). The particular design of [^{89}Zr]Zr-DFO-Gal3-F(ab')₂, a protein formed of two F(ab') fragments, results in faster blood clearance and lower liver uptake than traditional mAb-based tracers [125]. The high uptake of [^{89}Zr]Zr-DFO-Gal3-F(ab')₂ in kidneys is due to the urinary excretion [125], which should not be problematic because metastatic TC to the kidney is very rare [126]. For a diagnostic purpose, the dose is usually quite low and so is the nephrotoxicity. Thus [^{89}Zr]Zr-DFO-

Gal3-F(ab')₂ might be an excellent candidate for translation into the preoperative evaluation and postoperative follow-up.

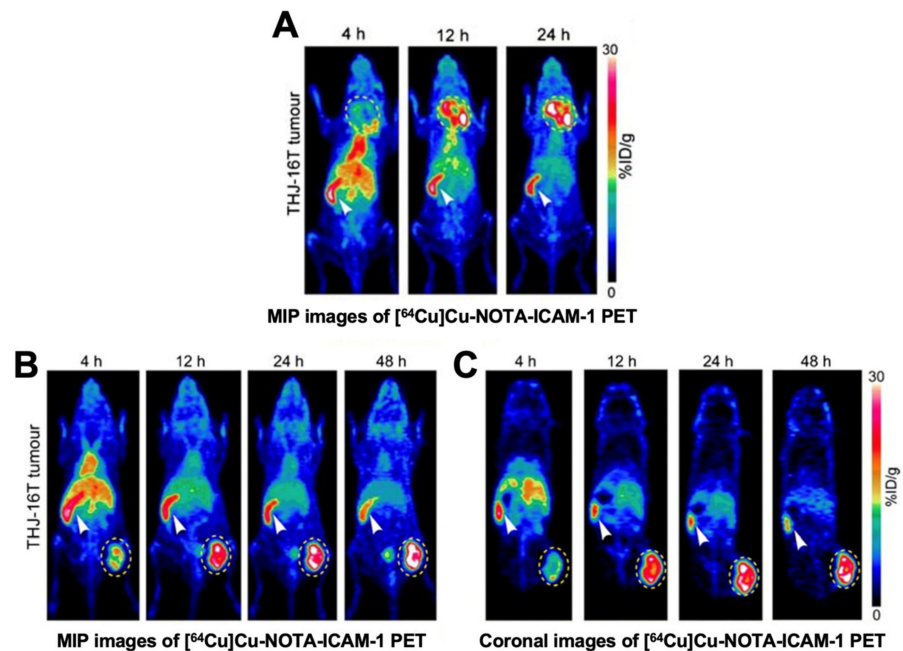


Figure 9. [⁶⁴Cu]Cu-NOTA-ICAM-1 immunoPET imaging in ATC xenografts (cell line: THJ-16T). (A) Maximum intensity projection (MIP) images in an orthotopic model. (B) MIP images in a subcutaneous model. (C) Coronal images of the same model. Reproduced with permission from [101], copyright 2020 Springer Nature Inc.

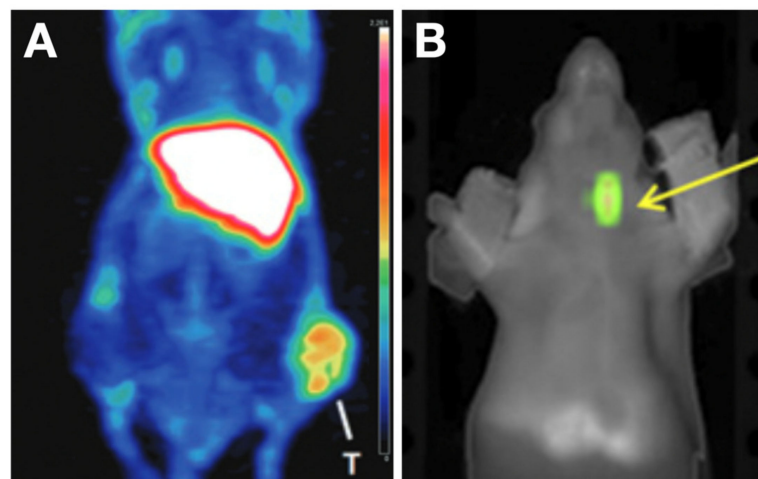


Figure 10. Characterization of [⁸⁹Zr]Zr-Gal-3 in TC xenografts. (A) PET image acquired at 48 h post radiotracer injection in a subcutaneous TC model showed an apparent accumulation of [⁸⁹Zr]Zr-Gal-3 in a tumor at the right thigh; Reproduced with permission from copyright 2016 American Association for Cancer Research [124]. (B) TC in an orthotopic model was visualized after injection of Cy5.5-Gal-3 with fluorescence imaging in the neck. Reproduced with permission from [125] copyright 2019 Society of Nuclear Medicine and Molecular Imaging.

4.2. Bispecific IgG Probes

Bispecific antibody (BsAb) probes have filled the vacancy of single target IgG probes in theranostics by providing higher antigen-binding capacity in tumor tissues than the monomeric counterparts [19]. Additionally, the pharmacokinetics of BsAbs could be improved by protein modification. The ability of BsAbs to bind to two targets allows these

bispecific IgG probes to display an enhanced role for targeting two antigens on a tumor cell surface, linking the tumor cells and immune cells, for instance [127,128]. However, until recently, only one BsAb targeting CEA and HSG has been thoroughly investigated in the diagnosis of MTC.

As stated previously, the intense expression of CEA is a biomarker of MTC. Prior clinical studies have shown the high sensitivity of the combination of anti-CEA BsAbs and ^{111}In or ^{131}I labeled haptens-peptides [129–131]. IMP288, an HSG hapten, was reported to have the ability to bind multiple radionuclides [132]. Meanwhile, a trivalent BsAb (called TF2), was engineered composing one HSG glycine Fab fragment and two anti-CEA Fab fragments [133]. The combination of ^{68}Ga labeled IMP288 and TF2 in PET imaging yields high sensitivity and specificity; Nevertheless, the pretargeting conditions may still need to be modified to reduce or avoid IMP288-induced adverse effects (malaise, bronchospasm, tachycardia, and hypertension) [132,134]. The delivery method of the tracer may challenge patients' acceptability because the combination of IMP288 and TF2 requires two injections: the first injection for TF2 BsAb, and a second injection for ^{68}Ga IMP288, with a time lag (one or two days) between the two injections [134] (Figure 11). The pretargeting strategy was used for the diagnostic purpose in the study. Replacement of ^{68}Ga with beta-emitter (e.g., ^{177}Lu) or alpha-emitter (e.g., ^{225}Ac) will further develop pretargeting therapeutic strategies, which will hopefully maximize the therapeutic index and minimize the adverse effects.

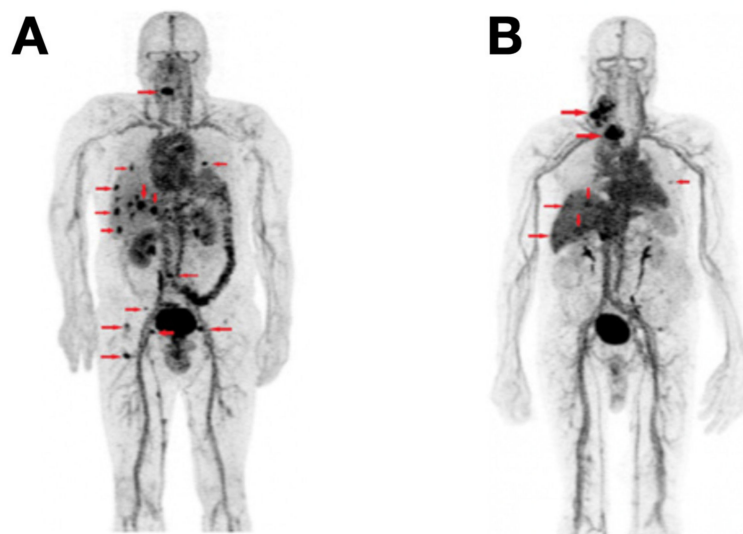


Figure 11. ^{68}Ga IMP288 plus TF2 PET revealed a considerable number of MTC foci. (A) Patient #1: foci were detected in multiple places, including supradiaphragmatic nodes, lung, liver, and bone, etc. (B) Patient #2: foci were detected in supradiaphragmatic nodes and liver, etc. Reproduced with permission from [134], copyright 2016 Society of Nuclear Medicine and Molecular Imaging.

4.3. Fab-Based Probes

Fab is characterized by a light chain and a heavy chain of an immunoglobulin, containing variable regions, constant domain of the light chain (CL), and first constant domain of the heavy chain (CH1) [135]. The Fab, therefore, takes the specificity of the immunoglobulin. Unlike the traditional antibodies (produced from mammalian cells), Fabs could be generally and easily produced from bacteria cells, like *E. coli* [136]. One drawback of Fab is the limited retention on the antigen and rapid clearance [137]. Some Fabs have been discovered for the treatment of TC (targeting cluster of differentiation 276 [CD276] [138], etc.), and some publications reported the potential value of Fab as diagnostic probes targeting Galectin-3 [125,139,140].

^{89}Zr Zr-DFO- αGal3 -Fab-PAS₂₀₀, an immunoPET probe fused with 200 Pro, Ala, and Ser residues (PAS₂₀₀) and conjugated with ^{89}Zr Zr-deferoxamine (^{89}Zr Zr-DFO), is a recently

reported Fab-based probe derived from the rat anti-Gal3 mAb. Similar to the full-size [^{89}Zr]/Zr-labeled Gal-3 mAb (mentioned in Section 4.1.3) [125], the [^{89}Zr]/Zr-DFO- α Gal3-Fab-PAS₂₀₀ can bind the Gal-3 well [139] (Figure 12). Unlike the uptake of full-size ^{89}Zr -labeled Gal-3 mAb which lasts over five days after injection, the [^{89}Zr]/Zr-DFO- α Gal3-Fab-PAS₂₀₀ was supposed to have a shorter lasting time, but the exact time was undetermined [125]. Research concerning a head-to-head comparison between the anti-Gal3 IgG probe and the corresponding fragment probe is lacking.

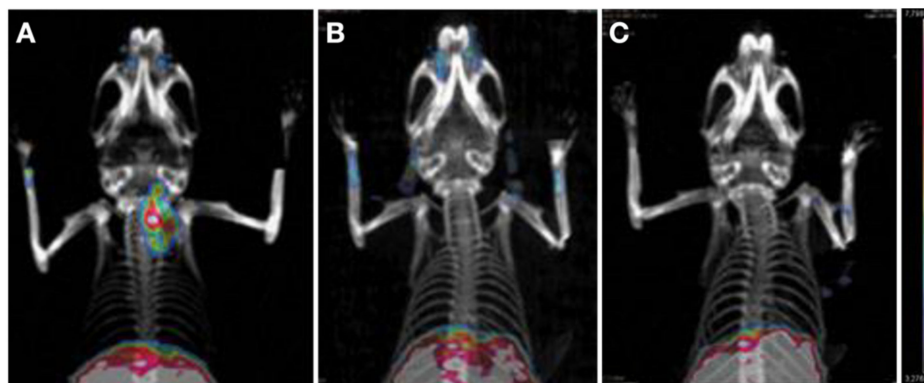


Figure 12. PET/CT images of mice at 24 h after intravenous injections. (A) Injection with 3 MBq of [^{89}Zr]/Zr-DFO- α Gal3-Fab-PAS₂₀₀. (B) Co-injection of 3 MBq of [^{89}Zr]/Zr-DFO- α Gal3-Fab-PAS₂₀₀ and 1000-fold of nonradioactive α Gal3-Fab-PAS₂₀₀ (for blocking). (C) Control. Color scale bars: 3.3–7.8%ID/g. Reproduced with permission from [139], copyright 2020 Mary Ann Liebert, Inc.

4.4. Nanobody-Based Probes

A single-domain antibody (sdAb, nanobody) is an engineered antibody fragment containing a single monomeric variable antibody domain. Compared to the large size of full-size antibodies (~150 kDa), nanobodies (~15 kDa) can be delivered to tumors with comparatively less obstruction [141]. Nanobodies can be reconstructed to Fc-domains or conjugated to molecular inhibitors, radioisotopes, fluorescent dye, and nanoparticles, making them suitable for targeting tumors with many applications [142]. For example, Jailkhani et al. established nanobody libraries against extracellular matrix (ECM) proteins, which are hallmarks of many diseases, including cancers. PET/CT imaging showed that ^{64}Cu -labeled NJB2 nanobody probes targeted ECM and detected breast cancer and melanoma for primary and metastatic foci (including thyroid) with excellent contrast [143]. Thus, nanobody probes may open up a promising opportunity for application in TCs. So far, nanobody probes remain absent in TC research [144]. Our team has developed a series of nanobodies targeting various targets (e.g., tumor-associated calcium signal transducer 2 [TACSTD2, TROP-2], ICAM-1, integrin associated protein [CD47], and melanoma cell adhesion molecule [MCAM, CD146]) and are fully exploring the theranostic potential of the nanobodies in TCs.

5. Other Probes

5.1. Aptamer-Based Probes

Aptamers are nucleic acids with antigen selectivity rivaling that of antibodies [145]. They bind to their target through electrostatic interactions, hydrophobic interactions, and induced fitting. Aptamers also offer target recognition that is comparable to traditional antibodies. Unlike antibodies, however, aptamers can be produced more feasibly. Its additional advantages include favorable storage properties and limited immunogenicity in vivo [146]. The major drawback of aptamers is the lack of stability in vivo. Regarding their application in TC, only a few aptamer probes have been reported [15].

5.1.1. Prominin 1 (PROM1, CD133)-Targeting Probes

CD133 is a kind of glycoprotein mainly expressed in hematopoietic stem and progenitor cells [147]. As a marker of cancer stem cells of brain tumor, colon cancer, melanoma, and ATCs [148–151], it is known to be responsible for the rapid growth of ATC and PTC cells [152,153]. Ge et al. synthesized and characterized an aptamer AP-1-M targeting CD133 in an ATC xenograft model. The synthesized AP-1-M-doxorubicin conjugates can effectively bind CD133-expressing tumor cells, and an intense signal may reflect the tumor proliferation at a fast pace [15] (Figure 13).

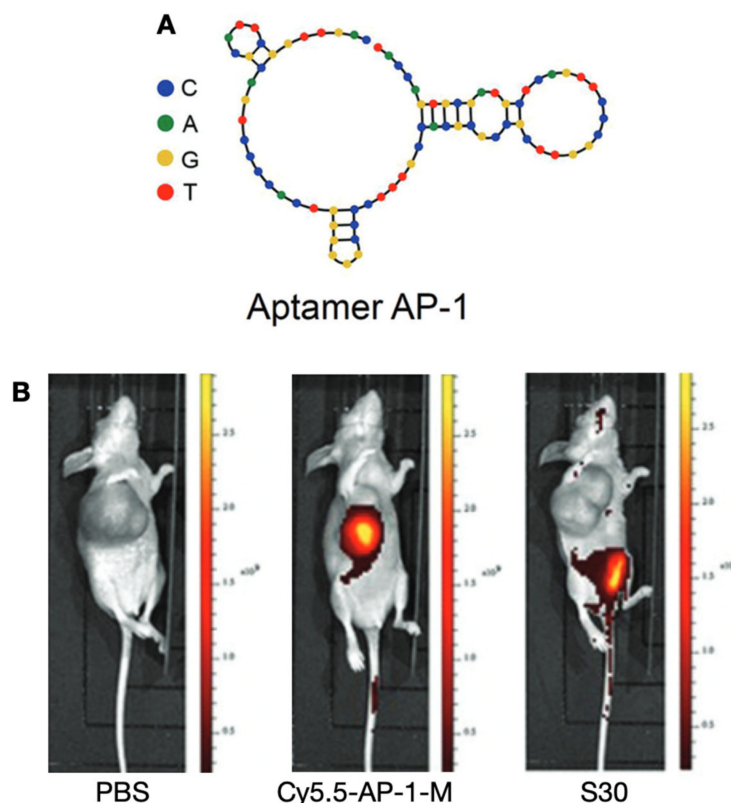


Figure 13. (A) Predicated structure of aptamer precursor AP-1. (B) Distribution of AP-1-M in a FRO xenograft model on fluorescence imaging at 48 h post-injection of PBS, Cy5.5-labeled AP-1-M, and control aptamer S30. Reproduced with permission from [15], copyright 2013 Royal Society of Chemistry.

5.1.2. PTC Tissue-Targeting Probes

Zhong et al. generated a PTC tissue-specific aptamer (TC-6) via tissue-based systematic evolution of ligands by exponential enrichment (SELEX), with clinical PTC tissues (positive control) and non-tumor thyroid tissues (negative control). The TC-6 can specifically distinguish PTC from other non-tumor tissues (Figure 14), and suppress the migration and invasion of PTC cells [16]. However, the exact molecular target remains unknown.

5.2. Nanoparticles-Based Probes

Nanoparticles have been emerging with widespread attention in MI, drug delivery, and disease treatment. Nanoparticles have brought their potential as MI agents to TC, primarily through their applicability in fluorescence imaging, ultrasound, and MRI [154,155]. These modalities enable nanoparticles to accumulate in cells by activation through US, light, temperature, and pH change, depending on the nanoparticle structures and their surface molecules. The ligand options for targeted nanoparticles are somewhat limited. Antibodies and peptides are the primary ligand choices due to their specific affinity to targets in TC fields. Although applications of targeted nanoparticles in TC have so far been limited,

there have been publications investigating nanoparticles conjugated to antibodies targeting epidermal growth factor receptor (EGFR) or Src homology 2 (SH2) domain-containing phosphatase 2 (SHP2) [154,155].

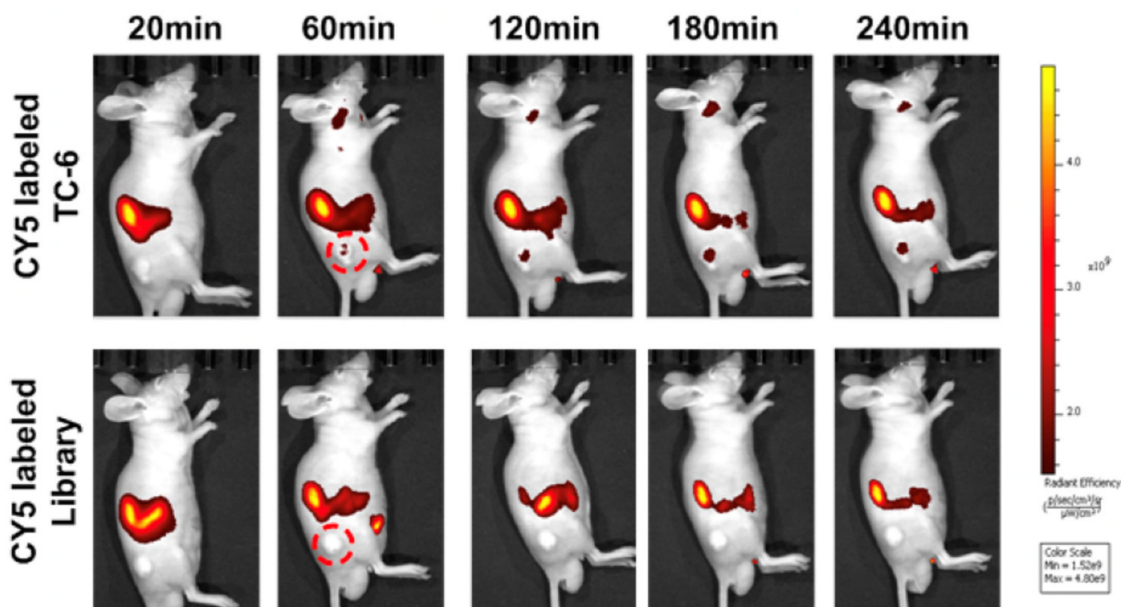


Figure 14. Time-lapse fluorescence imaged post-injection of Cy5-labeled TC-6 (**upper**) or library control (**lower**) in a TPC1 xenograft model. Reproduced with permission from [16], copyright 2016 American Association for Cancer Research.

5.2.1. EGFR-Targeting Probes

EGFR is a receptor binding the extracellular epidermal growth factor family (EGF family) [156]. In many tumor types, including TC, increased EGFR expression or activity initiates the tumor cell progression [112]. Recently, EGFR has been the target of the newly created nanoparticle (called C-HPNs) based on a core-shell system loaded with EGFR-targeted cetuximab and 10-hydroxycamptothecin (10-HCPT, chemotherapy agent). The EGFR antibody ligands enable nanoparticles to attach to cells which overexpress EGFR. With low-intensity focused ultrasound (LIFU) assistance, the liquid perfluoropentane (PFP) core in the nanoparticles would become vaporized and transformed into microbubbles, enhancing ultrasound contrast for tumor diagnosing. The core explosion induced by PFP boiling causes the release of 10-HCPT, providing more targeted delivery of the chemotherapeutic drug [154] (Figure 15).

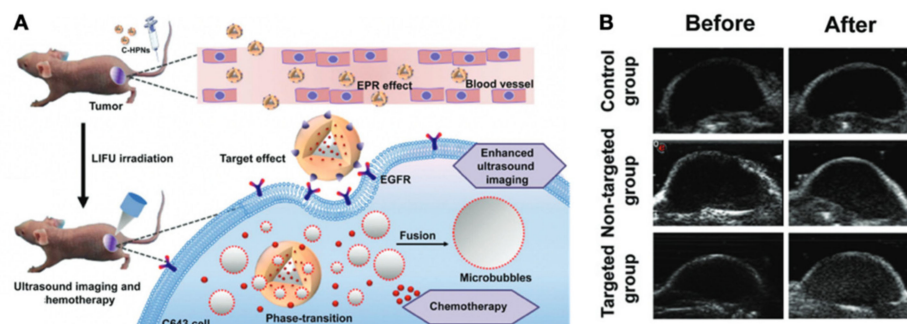


Figure 15. Theranostic applications of nanoparticles targeting EGFR. (A) Schematic illustration of the nanoparticles for chemotherapy drug delivery and enhanced diagnosis via LIFU. (B) Ultrasound imaging of tumors in B-mode before and after LIFU treatments. Reproduced with permission from [154], copyright 2019 Royal Society of Chemistry.

5.2.2. Protein Tyrosine Phosphatase Non-Receptor Type 11 (PTPN11, SHP2)-Targeting Probes

Another example is the SHP2, which is a tumor biomarker, acting as a signal of cell proliferation and immortality [157]. Hu et al. created an SHP2-targeted core-shell nanoparticle chelated with the contrast agent Gd^{3+} on the surface (NPs-SHP2). Similar to the EGFR-targeted nanoparticles mentioned previously, PFP-based LIFU can facilitate the probe carrying contrast agent been accumulated in the thyroid tumor area for enhanced MRI [155] (Figure 16).

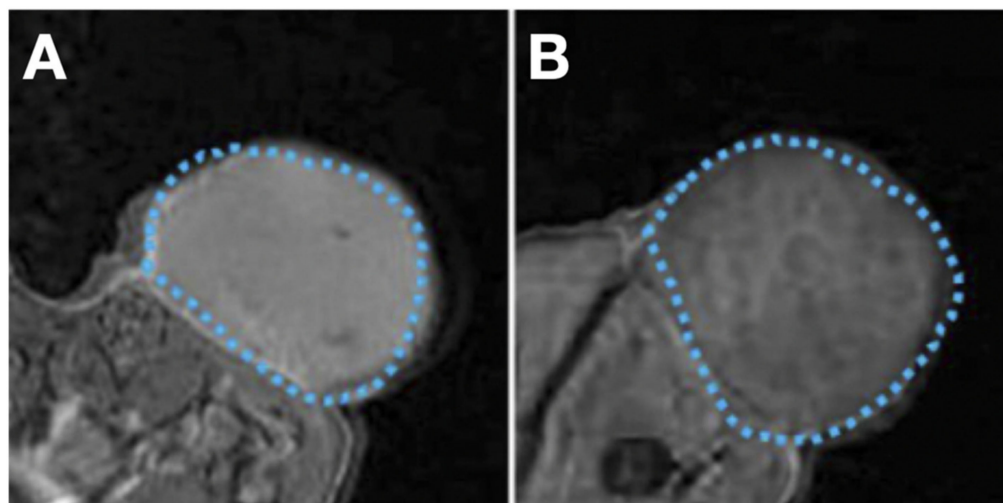


Figure 16. MRI in subcutaneous thyroid squamous cell cancer (TSCC) xenograft (blue dashed line) with NPs-SHP2 nanoparticles after LIFU treatment. (A) injection of SHP2-targeted nanoparticles. (B) injection of non-targeted nanoparticles (control). Reproduced with permission from [155], copyright Dove Medical Press Inc.

6. Conclusions and Future Perspectives

In summary, MI plays a vital role in evaluating and managing TCs, especially in accurately finding occult foci that are undetected by traditional ultrasound, CT, and MRI, thereby helping TC patients get the precise therapeutics (Table 1). Transporter-based probes tend to have high sensitivity, and immune-based probes generally have high specificity. So far, there is no single probe to reveal all the lesions both specifically and sensitively. Moreover, although TCs can be classified in a single pathological category, the biomarker expression in TC can vary dramatically. The apparent heterogeneity of TC requires the availability of more than one therapeutic method. By fully elucidating the biological characteristics of TCs and thoroughly exploring the biomarkers enriched in TCs [26,158,159], we believe that we can discover helpful targets for developing diagnostic probes and companion therapeutic agents for different molecular types of TC, not limited to pathological typing and phenotyping.

Table 1. A synoptic view of the MI radiotracers and their potential clinical value.

Tracer Types	Target	TC Type	Typical Roles	LoE [Ref.]
Transporter-targeting probes				
$[^{124}I]NaI$, $[^{131}I]NaI$	NIS	DTC	LL, TS, PE, TT, RD	Clinical [35,36]
$[^{18}F]TFB$, $[^{18}F]FS$, $[^{18}F]HFP$	NIS	DTC	LL, TS, PE, IUE	Clinical [50,51]
$[^{18}F]FDG$	GLUT1	TC	LL, TS, PE, PIU	Clinical [5,54,55]
$[^{18}F]FDOPA$	SLC7A5, SLC7A8	MTC	LL, TS, PE	Clinical [59,65]
$[^{11}C]MET$	SLC7A5	FTC	LL, TS, PE	Clinical [63]
$[^{18}F]FGln$	SLC7A5, SLC1A5, SLC38A1	PTC	LL, TS, PE	Clinical [62]
$[^{18}F]FLT$	ENT1	DTC	LL, TS, PE	Clinical [79,160]

Table 1. Cont.

Tracer Types	Target	TC Type	Typical Roles	LoE [Ref.]
Peptide-based probes				
⁶⁸ Ga/ ¹⁷⁷ Lu/ ⁹⁰ Y/ ¹¹¹ In labelled somatostatin analogue	SSTRs	TC	LL, TS, PE, PRRT	Clinical [161–163]
⁶⁸ Ga/ ¹⁷⁷ Lu labelled RGD ₂	αvβ3	TC	LL, TS, PE, PRRT	Clinical [85,86]
⁶⁸ Ga/ ¹⁷⁷ Lu labelled PSMA-ligand	PSMA	DTC	LL, TS, PE, PRRT	Clinical [88,91,164,165]
⁶⁸ Ga/ ¹⁷⁷ Lu labelled MGS5	CCK2R	MTC	LL, TS, PE, PRRT	Clinical [96] and preclinical [95]
Antibody-based probes				
Single target IgG-based probes				
⁸⁹ Zr or RDye 800CW labeled pertuzumab	HER2	ATC	LL, TS	Preclinical [114]
⁶⁴ Cu or RDye 800CW labeled ICAM-1 Ab	ICAM-1	ATC	LL, TS	Preclinical [101]
⁸⁹ Zr labeled Gal3 Ab	Gal3	DTC	LL, TS	Preclinical [124]
Bispecific IgG-based probes				
⁶⁸ Ga/ ¹⁷⁷ Lu labelled IMP288 plus TF2 BsAb	CEA × HSG	MTC	LL, TS, PE, PRRT	Clinical [134,166]
Fab-based probes				
⁸⁹ Zr or Cy5.5 labeled αGal3-Fab	Gal3	DTC	LL, TS	Preclinical [125,139,140]
Nanobody-based probes				
Targeting TROP-2 probes	TROP-2	TC (SP [167])	LL, TS, PRRT	Preclinical (OS)
Targeting CD47 probes	CD47	TC (SP [168])	LL, TS, PRRT	Preclinical (OS)
Targeting CD146 probes	CD146	TC (SP [169])	LL, TS, PRRT	Preclinical (OS)
Other probes				
Aptamer-based probes				
Cy5.5-AP-1-M	CD133	ATC	LL, TS	Preclinical [15]
Cy5-TC-6	PTC tissue	PTC	LL, TS	Preclinical [16]
Nanoparticles-based probes				
C-HPNs	EGFR	ATC	LL, TS, TT	Preclinical [154]
NPs-SHP2	SHP2	TC	LL, TS	Preclinical [155]

MI, molecular imaging; SP, speculative; LoE, level of evidence; LL, lesion localization; PE, prognosis evaluation; TT, tumor therapy; RD, radioiodine-131 dosimetry, [¹³¹I]NaI dosimetry; TS, tumor staging; IUE, iodine uptake evaluation; PIU, predicting iodine uptake; OS, ongoing study; PRRT, pre-evaluation for receptor radionuclide therapy; TC, thyroid cancer; PTC, papillary thyroid cancer; MTC, medullary thyroid cancer; ATC, anaplastic thyroid cancer; DTC, differentiated thyroid cancer; BsAb, bispecific antibody; Ab, antibody; Fab, antigen-binding fragment.

With the development of biological techniques and imaging tools, more valuable imaging methods are emerging. Integration of multiple imaging modalities and anatomical features would help physicians diagnose and treat TCs in a timely target-specific manner. Nanoparticles may enable anti-TC drug delivery and multimodality imaging, which may further improve the management of TC. However, the authors are cautious because of the limited clinical evidence in the field of TC. Bispecific MI probes have gained more traction in the past decade. The synthesis of bispecific antibody or antibody fragment tracers has been thoroughly elucidated elsewhere [170]. The importance of bispecific probes is that they enable enhanced affinity and high image quality, providing the ability targeting more occult foci than traditional single-target probes, and inducing more comprehensive application across TC patients with complex biological characteristics.

For antibody probe design, the traditional antibody-based radioactive or fluorescent probes for TCs have simply been prepared by non-selective conjugation on lysine/cysteine residues with or without chelators [171,172]. This approach may reduce target binding affinity, especially at a high conjugate/protein ratio, and in any case, leads to a mixture of products with different numbers of tags per protein molecule [173]. The method may also cause undesirable biodistribution (e.g., high kidney uptake and poor tumor targeting due to *in vivo* cleavage of the S–S linkage) and pharmacokinetics (fast antibody clearance for modification of interchain disulfide cysteine) [174]. Protein engineering techniques are progressing very rapidly. In this setting, the site-specific and homogeneous introduction of the tags into the targeting moieties would be more advantageous. The emerging techniques mainly include chelator conjunction to the antibody glycan region, enzyme-assisted chelator attachment, and incorporating and chelating radioisotope into amino acid sequences [171]. This may help us design molecular imaging agents and companion therapeutic agents with increased possibility for clinical translation.

For the diagnosis of TC, the superiority of MI over conventional anatomical imaging is clear, with advantages of favorable spatial and temporal resolution and functional imaging [175]. The emergence of MI has fundamentally changed the management of TC. For instance, [¹⁸F]FDG PET/CT plays its role in optimizing initial therapy, which is mandatory for improving DTC outcome. [¹⁸F]FDG PET/CT could be conducted if some foci are radioiodine non-avid before treatment planning. Rosenbaum-Krumme et al. found that the TNM staging and management were changed from standard therapy (surgery plus ¹³¹I therapy) to individual therapy (standard therapy plus external beam therapy or targeted therapy etc.) because of the [¹⁸F]FDG PET/CT results in 21% of the high-risk DTCs [176]. We suppose that MI in TCs would become a helpful modality for tumor staging, prognosis evaluation, which may lead to immense changes in what treatments the TC patients are given, maximizing the benefits of individual therapy.

For TC therapy, despite the rapid progress in molecular imaging, we firmly believe that the innovation of therapeutic agents should accompany the development of diagnostic agents. For example, radionuclides such as ¹⁷⁷Lu, ²²⁵Ac, ¹⁸⁸Re, ⁶⁷Cu, ⁴⁷Sc, ¹⁶⁶Ho, ⁹⁰Y, ¹⁶¹Tb, ¹⁴⁹Tb, ²¹²Pb, and ²¹³Bi emitting α -particles, β -particles, and Auger electrons can be feasibly chelated with DOTA, NOTA, etc., which is similar to the diagnostic isotopes mentioned in this review, ⁶⁴Cu or ⁶⁸Ga chelated with NOTA or DOTA [177]. For theranostic application, diagnostic probes with a chelating agent and a radionuclide suitable for imaging (e.g., NOTA and ⁶⁴Cu) can be used to map the target and assess the therapeutic potential of the same probe labelled with the same chelating agent and a therapeutic radionuclide (e.g., NOTA and ⁶⁷Cu) [19]. ¹⁴⁹Tb is another theranostic radioisotope that has not been investigated in thyroid cancer research to date. ¹⁴⁹Tb can simultaneously emit positrons (β^+ particles), α -particles, and γ -radiation, allowing PET and α particle-based therapy to go on at the same time [177]. The current review focuses on emerging probes for imaging with examples. Further introduction and discussion about the concept of TC therapy or theranostics will be updated and illustrated in an upcoming review. We hope the ever-developing diagnostic and therapeutic probes and theranostic applications can substantially improve the management of TCs, especially the aggressive RR-DTCs, MTCs, and ATCs.

In the last two decades, there has been a general increase in the prevalence of TC. The phenomenon is partially due to environmental factors (e.g., chemical pollution, anthropogenic or natural radiation), but is also due to overdiagnosis by increased screening with more sensitive methods (e.g., high-resolution ultrasound), especially in developed countries (e.g., South Korea and the United States), leading to unnecessary treatment. As mentioned previously, most incident TCs are low-risk DTCs that tend to retain their stability over the years until death due to aging. Therefore, it is unnecessary to treat indolent TCs because of the low cost-effectiveness and the practically unchanged mortality. Something to note is that the ever-developing MI techniques might more sensitively detect TCs, potentially causing overdiagnosis for indolent TC and overtreatment via invasive methods (e.g.,

thyroidectomy or metastasectomy) or noninvasive therapeutics (e.g., chemotherapy agents or multikinase inhibitors). To avoid these pitfalls, future work could focus on discovering prognosis- or progress-related targets or probes, thereby classifying TCs into indolent and active disease. In other words, future MI research should not be limited to the field of finding latent TC lesions.

Author Contributions: Conceptualization, Y.J., W.W. and W.C.; Methodology, Y.J., B.L. and W.W.; Writing—original draft preparation, Y.J.; Writing—review and editing, B.L., M.H.Y. and W.W.; Visualization, Y.J.; Supervision, W.W. and W.C.; Project administration, W.W. and W.C.; Funding acquisition, W.W., W.C., J.L. and G.H. All authors have read and agreed to the published version of the manuscript.

Funding: This research was funded by the National Key Research and Development Program of China (grant no. 2020YFA0909000), the National Natural Science Foundation of China (grant no. 82001878), the Shanghai Rising-Star Program (Grant No. 20QA1406100), and the University of Wisconsin–Madison. Y.J. is supported by a postgraduate scholarship from the China Scholarship Council.

Institutional Review Board Statement: Not applicable.

Informed Consent Statement: Not applicable.

Data Availability Statement: No new data were created or analyzed in this study. Data sharing is not applicable to this article.

Conflicts of Interest: Weibo Cai is a scientific advisor, stockholder, and grantee of Focus-X Therapeutics, Inc. All other authors declare no conflict of interest.

References

- Lim, H.; Devesa, S.S.; Sosa, J.A.; Check, D.; Kitahara, C.M. Trends in Thyroid Cancer Incidence and Mortality in the United States, 1974–2013. *JAMA* **2017**, *317*, 1338. [[CrossRef](#)] [[PubMed](#)]
- Chen, W.; Zheng, R.; Baade, P.D.; Zhang, S.; Zeng, H.; Bray, F.; Jemal, A.; Yu, X.Q.; He, J. Cancer Statistics in China, 2015. *CA Cancer J. Clin.* **2016**, *66*, 115–132. [[CrossRef](#)] [[PubMed](#)]
- Rahib, L.; Smith, B.D.; Aizenberg, R.; Rosenzweig, A.B.; Fleshman, J.M.; Matrisian, L.M. Projecting Cancer Incidence and Deaths to 2030: The Unexpected Burden of Thyroid, Liver, and Pancreas Cancers in the United States. *Cancer Res.* **2014**, *74*, 2913–2921. [[CrossRef](#)] [[PubMed](#)]
- De la Vieja, A.; Riesco-Eizaguirre, G. Radio-Iodide Treatment: From Molecular Aspects to the Clinical View. *Cancers* **2021**, *13*, 995. [[CrossRef](#)] [[PubMed](#)]
- Haugen, B.R.; Alexander, E.K.; Bible, K.C.; Doherty, G.M.; Mandel, S.J.; Nikiforov, Y.E.; Pacini, F.; Randolph, G.W.; Sawka, A.M.; Schlumberger, M.; et al. 2015 American Thyroid Association Management Guidelines for Adult Patients with Thyroid Nodules and Differentiated Thyroid Cancer: The American Thyroid Association Guidelines Task Force on Thyroid Nodules and Differentiated Thyroid Cancer. *Thyroid* **2016**, *26*, 1–133. [[CrossRef](#)]
- Schlumberger, M.; Leboulleux, S. Current Practice in Patients with Differentiated Thyroid Cancer. *Nat. Rev. Endocrinol.* **2021**, *17*, 176–188. [[CrossRef](#)]
- Durante, C.; Haddy, N.; Baudin, E.; Leboulleux, S.; Hartl, D.; Travagli, J.P.; Caillou, B.; Ricard, M.; Lumbroso, J.D.; Vathaire, F.D.; et al. Long-Term Outcome of 444 Patients with Distant Metastases from Papillary and Follicular Thyroid Carcinoma: Benefits and Limits of Radioiodine Therapy. *J. Clin. Endocrinol. Metab.* **2006**, *91*, 2892–2899. [[CrossRef](#)]
- ACS Thyroid Cancer Survival Rates, by Type and Stage. Available online: <https://www.cancer.org/cancer/thyroid-cancer/detection-diagnosis-staging/survival-rates.html> (accessed on 5 June 2021).
- Lin, B.; Ma, H.; Ma, M.; Zhang, Z.; Sun, Z.; Hsieh, I.-Y.; Okenwa, O.; Guan, H.; Li, J.; Lv, W. The Incidence and Survival Analysis for Anaplastic Thyroid Cancer: A SEER Database Analysis. *Am. J. Transl. Res.* **2019**, *11*, 5888–5896.
- James, M.L.; Gambhir, S.S. A Molecular Imaging Primer: Modalities, Imaging Agents, and Applications. *Physiol. Rev.* **2012**, *92*, 897–965. [[CrossRef](#)]
- Wahl, R.L.; Chareonthaitawee, P.; Clarke, B.; Drzezga, A.; Lindenberg, L.; Rahmim, A.; Thackeray, J.; Ulaner, G.A.; Weber, W.; Zukotynski, K.; et al. Mars Shot for Nuclear Medicine, Molecular Imaging, and Molecularly Targeted Radiopharmaceutical Therapy. *J. Nucl. Med. Off. Publ. Soc. Nucl. Med.* **2021**, *62*, 6–14. [[CrossRef](#)]
- Piccardo, A.; Trimboli, P.; Foppiani, L.; Treglia, G.; Ferrarazzo, G.; Massollo, M.; Bottoni, G.; Giovanella, L. PET/CT in Thyroid Nodule and Differentiated Thyroid Cancer Patients. The Evidence-Based State of the Art. *Rev. Endocr. Metab. Disord.* **2019**, *20*, 47–64. [[CrossRef](#)]

13. Kendler, D.B.; Araújo, M.L., Jr.; Alencar, R.; Accioly, M.T.D.S.; Bulzico, D.A.; Pessoa, C.C.D.N.; Accioly, F.A.; De Farias, T.P.; Lopes, F.P.P.L.; Corbo, R.; et al. Somatostatin Receptor Subtype 1 Might Be a Predictor of Better Response to Therapy in Medullary Thyroid Carcinoma. *Endocrine* **2017**, *58*, 474–480. [[CrossRef](#)]
14. Ambrosini, V.; Kunikowska, J.; Baudin, E.; Bodei, L.; Bouvier, C.; Capdevila, J.; Cremonesi, M.; de Herder, W.W.; Dromain, C.; Falconi, M.; et al. Consensus on Molecular Imaging and Theranostics in Neuroendocrine Neoplasms. *Eur. J. Cancer* **2021**, *146*, 56–73. [[CrossRef](#)]
15. Ge, M.H.; Zhu, X.H.; Shao, Y.M.; Wang, C.; Huang, P.; Wang, Y.; Jiang, Y.; Maimaitiyiming, Y.; Chen, E.; Yang, C.; et al. Synthesis and Characterization of CD133 Targeted Aptamer–Drug Conjugates for Precision Therapy of Anaplastic Thyroid Cancer. *Biomater. Sci.* **2020**. [[CrossRef](#)]
16. Zhong, W.; Pu, Y.; Tan, W.; Liu, J.; Liao, J.; Liu, B.; Chen, K.; Yu, B.; Hu, Y.; Deng, Y.; et al. Identification and Application of an Aptamer Targeting Papillary Thyroid Carcinoma Using Tissue-SELEX. *Anal. Chem.* **2019**, *91*, 8289–8297. [[CrossRef](#)]
17. Zhu, C.; Li, L.; Fang, S.; Zhao, Y.; Zhao, L.; Yang, G.; Qu, F. Selection and Characterization of an SsDNA Aptamer against Thyroglobulin. *Talanta* **2021**, *223*, 121690. [[CrossRef](#)]
18. Kumarasamy, J.; Ghorui, S.K.; Gholve, C.; Jain, B.; Dhekale, Y.; Gupta, G.D.; Damle, A.; Banerjee, S.; Rajan, M.G.R.; Kulkarni, S. Production, Characterization and in-Vitro Applications of Single-Domain Antibody against Thyroglobulin Selected from Novel T7 Phage Display Library. *J. Immunol. Methods* **2021**, *492*, 112990. [[CrossRef](#)]
19. Wei, W.; Rosenkrans, Z.T.; Liu, J.; Huang, G.; Luo, Q.-Y.; Cai, W. ImmunoPET: Concept, Design, and Applications. *Chem. Rev.* **2020**, *120*, 3787–3851. [[CrossRef](#)]
20. Achmad, A.; Bhattarai, A.; Yudistiro, R.; Heryanto, Y.D.; Higuchi, T.; Tsushima, Y. The Diagnostic Performance of 18F-FAMT PET and 18F-FDG PET for Malignancy Detection: A Meta-Analysis. *BMC Med. Imaging* **2017**, *17*, 66. [[CrossRef](#)]
21. Enomoto, K.; Hotomi, M. Amino Acid Transporters as Potential Therapeutic Targets in Thyroid Cancer. *Endocrinol. Metab.* **2020**, *35*, 227–236. [[CrossRef](#)]
22. Fu, H.; Sa, R.; Cheng, L.; Jin, Y.; Qiu, X.; Liu, M.; Chen, L. An updated review on nuclear molecular imaging of thyroid cancers. *Endocr. Pract.* **2020**, *27*, 494–502. [[CrossRef](#)] [[PubMed](#)]
23. Portulano, C.; Paroder-Belenitsky, M.; Carrasco, N. The Na⁺/I[−] Symporter (NIS): Mechanism and Medical Impact. *Endocr. Rev.* **2013**, *35*, 106–149. [[CrossRef](#)] [[PubMed](#)]
24. Mariani, G.; Tonacchera, M.; Grosso, M.; Orsolini, F.; Vitti, P.; Strauss, H.W. The Role of Nuclear Medicine in the Clinical Management of Benign Thyroid Disorders, Part 1: Hyperthyroidism. *J. Nucl. Med.* **2021**, *62*, 304–312. [[CrossRef](#)] [[PubMed](#)]
25. Oh, J.M.; Ahn, B.-C. Molecular Mechanisms of Radioactive Iodine Refractoriness in Differentiated Thyroid Cancer: Impaired Sodium Iodide Symporter (NIS) Expression Owing to Altered Signaling Pathway Activity and Intracellular Localization of NIS. *Theranostics* **2021**, *11*, 6251–6277. [[CrossRef](#)] [[PubMed](#)]
26. Jin, Y.; Nostrand, D.V.; Cheng, L.; Liu, M.; Chen, L. Radioiodine Refractory Differentiated Thyroid Cancer. *Crit. Rev. Oncol. Hemat.* **2018**, *125*, 111–120. [[CrossRef](#)] [[PubMed](#)]
27. Nagarajah, J.; Janssen, M.; Hetkamp, P.; Jentzen, W. Iodine Symporter Targeting with 124 I/ 131 I Theranostics. *J. Nucl. Med.* **2017**, *58*, 34S–38S. [[CrossRef](#)]
28. Wyszomirska, A. Iodine-131 for Therapy of Thyroid Diseases. Physical and Biological Basis. *Nucl. Med. Rev. Cent. East. Eur.* **2012**, *15*, 120–123.
29. Gulec, S.A.; Kuker, R.A.; Goryawala, M.; Fernandez, C.; Perez, R.; Khan-Ghany, A.; Apaza, A.; Harja, E.; Harrell, M. 124 I PET/CT in Patients with Differentiated Thyroid Cancer: Clinical and Quantitative Image Analysis. *Thyroid* **2016**, *26*, 441–448. [[CrossRef](#)]
30. Jentzen, W.; Verschure, F.; van Zon, A.; van de Kolk, R.; Wierts, R.; Schmitz, J.; Bockisch, A.; Binse, I. 124I PET Assessment of Response of Bone Metastases to Initial Radioiodine Treatment of Differentiated Thyroid Cancer. *J. Nucl. Med.* **2016**, *57*, 1499–1504. [[CrossRef](#)]
31. Ruhlmann, M.; Jentzen, W.; Ruhlmann, V.; Pettinato, C.; Rossi, G.; Binse, I.; Bockisch, A.; Rosenbaum-Krumme, S. High Level of Agreement Between Pretherapeutic 124I PET and Intratherapeutic 131I Imaging in Detecting Iodine-Positive Thyroid Cancer Metastases. *J. Nucl. Med.* **2016**, *57*, 1339–1342. [[CrossRef](#)]
32. Jin, Y.; Ruan, M.; Cheng, L.; Fu, H.; Liu, M.; Sheng, S.; Chen, L. Radioiodine Uptake and Thyroglobulin-Guided Radioiodine Remnant Ablation in Patients with Differentiated Thyroid Cancer: A Prospective, Randomized, Open-Label, Controlled Trial. *Thyroid* **2019**, *29*, 101–110. [[CrossRef](#)]
33. Simon, D.; Körber, C.; Krausch, M.; Segering, J.; Groth, P.; Görges, R.; Grünwald, F.; Müller-Gärtner, H.; Schmutzler, C.; Köhrle, J.; et al. Clinical Impact of Retinoids in Redifferentiation Therapy of Advanced Thyroid Cancer: Final Results of a Pilot Study. *Eur. J. Nucl. Med. Mol. Imaging* **2002**, *29*, 775–782. [[CrossRef](#)]
34. Plantinga, T.S.; Heinhuis, B.; Gerrits, D.; Netea, M.G.; Joosten, L.A.B.; Hermus, A.R.M.M.; Oyen, W.J.G.; Schweppe, R.E.; Haugen, B.R.; Boerman, O.C.; et al. MTOR Inhibition Promotes TTF1-Dependent Redifferentiation and Restores Iodine Uptake in Thyroid Carcinoma Cell Lines. *J. Clin. Endocrinol. Metab.* **2014**, *99*, E1368–E1375. [[CrossRef](#)]
35. Ho, A.L.; Grewal, R.K.; Leboeuf, R.; Sherman, E.J.; Pfister, D.G.; Deandreis, D.; Pentlow, K.S.; Zanzonico, P.B.; Haque, S.; Gavane, S.; et al. Selumetinib-Enhanced Radioiodine Uptake in Advanced Thyroid Cancer. *N. Engl. J. Med.* **2013**, *368*, 623–632. [[CrossRef](#)]
36. Dunn, L.A.; Sherman, E.J.; Baxi, S.S.; Tchekmedyan, V.; Grewal, R.K.; Larson, S.M.; Pentlow, K.S.; Haque, S.; Tuttle, R.M.; Sabra, M.M.; et al. Vemurafenib Redifferentiation of BRAF Mutant, RAI-Refractory Thyroid Cancers. *J. Clin. Endocrinol. Metab.* **2018**, *104*, 1417–1428. [[CrossRef](#)]

37. Vaisman, F.; Carvalho, D.P.; Vaisman, M. A New Appraisal of Iodine Refractory Thyroid Cancer. *Endocr. Relat. Cancer* **2015**, *22*, R301–R310. [[CrossRef](#)]
38. Misawa, A.; Inoue, S. Estrogen-Related Receptors in Breast Cancer and Prostate Cancer. *Front. Endocrinol.* **2015**, *6*, 83. [[CrossRef](#)]
39. Singh, T.D.; Jeong, S.Y.; Lee, S.-W.; Ha, J.-H.; Lee, I.-K.; Kim, S.H.; Kim, J.; Cho, S.J.; Ahn, B.-C.; Lee, J.; et al. Inverse Agonist of Estrogen-Related Receptor γ Enhances Sodium Iodide Symporter Function Through Mitogen-Activated Protein Kinase Signaling in Anaplastic Thyroid Cancer Cells. *J. Nucl. Med. Off. Publ. Soc. Nucl. Med.* **2015**, *56*, 1690–1696. [[CrossRef](#)]
40. Singh, T.D.; Song, J.; Kim, J.; Chin, J.; Ji, H.D.; Lee, J.-E.; Lee, S.B.; Yoon, H.; Yu, J.H.; Kim, S.K.; et al. A Novel Orally Active Inverse Agonist of Estrogen-Related Receptor Gamma (ERR γ), DN200434, A Booster of NIS in Anaplastic Thyroid Cancer. *Clin. Cancer Res.* **2019**, *25*, 5069–5081. [[CrossRef](#)]
41. Hershman, J.M. To Avoid Stunning, Give Treatment Doses of Radioiodine-131 within Three Days after Completing the Diagnostic Scan or Wait Seven Days. *Clin. Thyroid.* **2015**, *27*, 341–343. [[CrossRef](#)]
42. Silberstein, E.B.; Alavi, A.; Balon, H.R.; Clarke, S.E.M.; Divgi, C.; Gelfand, M.J.; Goldsmith, S.J.; Jadvar, H.; Marcus, C.S.; Martin, W.H.; et al. The SNMMI Practice Guideline for Therapy of Thyroid Disease with ¹³¹I 3.0. *J. Nucl. Med.* **2012**, *53*, 1633–1651. [[CrossRef](#)] [[PubMed](#)]
43. Silberstein, E.B. The Problem of the Patient with Thyroglobulin Elevation but Negative Iodine Scintigraphy: The TENIS Syndrome. *Semin. Nucl. Med.* **2011**, *41*, 113–120. [[CrossRef](#)] [[PubMed](#)]
44. Kim, M.J.; Sun, H.J.; Song, Y.S.; Yoo, S.-K.; Kim, Y.A.; Seo, J.-S.; Park, Y.J.; Cho, S.W. CXCL16 Positively Correlated with M2-Macrophage Infiltration, Enhanced Angiogenesis, and Poor Prognosis in Thyroid Cancer. *Sci. Rep.* **2019**, *9*, 13288. [[CrossRef](#)] [[PubMed](#)]
45. Jiang, H.; Bansal, A.; Goyal, R.; Peng, K.-W.; Russell, S.J.; DeGrado, T.R. Synthesis and Evaluation of ¹⁸F-Hexafluorophosphate as a Novel PET Probe for Imaging of Sodium/Iodide Symporter in a Murine C6-Glioma Tumor Model. *Bioorg. Med. Chem.* **2018**, *26*, 225–231. [[CrossRef](#)]
46. Jiang, H.; DeGrado, T.R. [¹⁸F]Tetrafluoroborate ([¹⁸F]TFB) and Its Analogs for PET Imaging of the Sodium/Iodide Symporter. *Theranostics* **2018**, *8*, 3918–3931. [[CrossRef](#)]
47. Dittmann, M.; Carvalho, J.M.G.; Rahbar, K.; Schäfers, M.; Claesener, M.; Riemann, B.; Seifert, R. Incremental Diagnostic Value of [¹⁸F]Tetrafluoroborate PET-CT Compared to [¹³¹I]Iodine Scintigraphy in Recurrent Differentiated Thyroid Cancer. *Eur. J. Nucl. Med. Mol. Imaging* **2020**, *47*, 2639–2646. [[CrossRef](#)]
48. Khoshnevisan, A.; Chuamsaamarkkee, K.; Boudjemline, M.; Jackson, A.; Smith, G.E.; Gee, A.D.; Fruhwirth, G.O.; Blower, P.J. ¹⁸F-Fluorosulfate for PET Imaging of the Sodium–Iodide Symporter: Synthesis and Biologic Evaluation In Vitro and In Vivo. *J. Nucl. Med.* **2017**, *58*, 156–161. [[CrossRef](#)]
49. Concilio, S.C.; Zhekova, H.R.; Noskov, S.Y.; Russell, S.J. Inter-Species Variation in Monovalent Anion Substrate Selectivity and Inhibitor Sensitivity in the Sodium Iodide Symporter (NIS). *PLoS ONE* **2020**, *15*, e0229085. [[CrossRef](#)]
50. O’Doherty, J.; Jauregui-Osoro, M.; Brothwood, T.; Szyzsko, T.; Marsden, P.K.; O’Doherty, M.J.; Cook, G.J.R.; Blower, P.J.; Lewington, V. ¹⁸F-Tetrafluoroborate, a PET Probe for Imaging Sodium/Iodide Symporter Expression: Whole-Body Biodistribution, Safety, and Radiation Dosimetry in Thyroid Cancer Patients. *J. Nucl. Med.* **2017**, *58*, 1666–1671. [[CrossRef](#)]
51. Samnick, S.; Al-Momani, E.; Schmid, J.-S.; Mottok, A.; Buck, A.K.; Lapa, C. Initial Clinical Investigation of [¹⁸F]Tetrafluoroborate PET/CT in Comparison to [¹²⁴I]Iodine PET/CT for Imaging Thyroid Cancer. *Clin. Nucl. Med.* **2018**, *43*, 162–167. [[CrossRef](#)]
52. Zhang, Y.; Wang, J. Targeting Uptake Transporters for Cancer Imaging and Treatment. *Acta Pharm. Sin. B* **2019**, *10*, 79–90. [[CrossRef](#)]
53. Nagarajah, J.; Ho, A.L.; Tuttle, R.M.; Weber, W.A.; Grewal, R.K. Correlation of BRAFV600E Mutation and Glucose Metabolism in Thyroid Cancer Patients: An ¹⁸F-FDG PET Study. *J. Nucl. Med.* **2015**, *56*, 662–667. [[CrossRef](#)]
54. Liu, M.; Cheng, L.; Jin, Y.; Ruan, M.; Sheng, S.; Chen, L. Predicting ¹³¹I-Avidity of Metastases from Differentiated Thyroid Cancer Using ¹⁸F-FDG PET/CT in Postoperative Patients with Elevated Thyroglobulin. *Sci. Rep.* **2018**, *8*, 4352. [[CrossRef](#)]
55. Kang, S.Y.; Bang, J.-I.; Kang, K.W.; Lee, H.; Chung, J.-K. FDG PET/CT for the Early Prediction of RAI Therapy Response in Patients with Metastatic Differentiated Thyroid Carcinoma. *PLoS ONE* **2019**, *14*, e0218416. [[CrossRef](#)]
56. Feng, H.; Wang, X.; Chen, J.; Cui, J.; Gao, T.; Gao, Y.; Zeng, W. Nuclear Imaging of Glucose Metabolism: Beyond ¹⁸F-FDG. *Contrast Media Mol. Imaging* **2019**, *2019*, 7954854. [[CrossRef](#)]
57. Galldiks, N.; Langen, K.-J.; Albert, N.L.; Chamberlain, M.; Soffietti, R.; Kim, M.M.; Law, I.; Rhun, E.L.; Chang, S.; Schwarting, J.; et al. PET Imaging in Patients with Brain Metastasis—Report of the RANO/PET Group. *Neuro-Oncology* **2019**, *21*, 585–595. [[CrossRef](#)]
58. Pagano, L.; Samà, M.T.; Morani, F.; Prodam, F.; Rudoni, M.; Boldorini, R.; Valente, G.; Marzullo, P.; Baldelli, R.; Appetecchia, M.; et al. Thyroid Incidentaloma Identified by ¹⁸F-Fluorodeoxyglucose Positron Emission Tomography with CT (FDG-PET/CT): Clinical and Pathological Relevance. *Clin. Endocrinol.* **2011**, *75*, 528–534. [[CrossRef](#)]
59. Giovannella, L.; Treglia, G.; Iakovou, I.; Mihailovic, J.; Verburg, F.A.; Luster, M. EANM Practice Guideline for PET/CT Imaging in Medullary Thyroid Carcinoma. *Eur. J. Nucl. Med. Mol. Imaging* **2020**, *47*, 61–77. [[CrossRef](#)]
60. Beheshti, M.; Pöcher, S.; Vali, R.; Waldenberger, P.; Broinger, G.; Nader, M.; Kohlfürst, S.; Pirich, C.; Dralle, H.; Langsteger, W. The Value of ¹⁸F-DOPA PET-CT in Patients with Medullary Thyroid Carcinoma: Comparison with ¹⁸F-FDG PET-CT. *Eur. Radiol.* **2009**, *19*, 1425–1434. [[CrossRef](#)]

61. Liu, F.; Xu, X.; Zhu, H.; Zhang, Y.; Yang, J.; Zhang, L.; Li, N.; Zhu, L.; Kung, H.F.; Yang, Z. PET Imaging of 18 F-(2S,4R)4-Fluoroglutamine Accumulation in Breast Cancer: From Xenografts to Patients. *Mol Pharm.* **2018**, *15*, 3448–3455. [[CrossRef](#)]
62. Xu, X.; Zhu, H.; Liu, F.; Zhang, Y.; Yang, J.; Zhang, L.; Xie, Q.; Zhu, L.; Li, N.; Kung, H.F.; et al. Dynamic PET/CT Imaging of 18F-(2S, 4R)4-Fluoroglutamine in Healthy Volunteers and Oncological Patients. *Eur. J. Nucl. Med. Mol. Imaging* **2020**, *47*, 2280–2292. [[CrossRef](#)]
63. Jochumsen, M.R.; Iversen, P.; Arveschoug, A.K. Follicular Thyroid Cancer Avid on C-11 Methionine PET/CT. *Endocrinol. Diabetes Metab. Case Rep.* **2018**, *2018*. [[CrossRef](#)]
64. Barollo, S.; Bertazza, L.; Watutantrige-Fernando, S.; Censi, S.; Cavedon, E.; Galuppini, F.; Pennelli, G.; Fassina, A.; Citton, M.; Rubin, B.; et al. Overexpression of L-Type Amino Acid Transporter 1 (LAT1) and 2 (LAT2): Novel Markers of Neuroendocrine Tumors. *PLoS ONE* **2016**, *11*, e0156044. [[CrossRef](#)]
65. Yang, J.H.; Camacho, C.P.; Lindsey, S.C.; Valente, F.O.F.; Andreoni, D.M.; Yamaga, L.Y.; Wagner, J.; Biscolla, R.P.M.; Maciel, R.M.B. The Combined Use of Calcitonin Doubling Time and 18F-FDG PET/CT Improves Prognostic Values in Medullary Thyroid Carcinoma: The Clinical Utility of 18F-FDG PET/CT. *Endocr. Pract.* **2017**, *23*, 942–948. [[CrossRef](#)]
66. Weber, T.; Gottstein, M.; Schwenzler, S.; Beer, A.; Luster, M. Is C-11 Methionine PET/CT Able to Localise Sestamibi-Negative Parathyroid Adenomas? *World J. Surg.* **2017**, *41*, 980–985. [[CrossRef](#)]
67. Yuan, L.; Liu, J.; Kan, Y.; Yang, J.; Wang, X. The Diagnostic Value of 11C-Methionine PET in Hyperparathyroidism with Negative 99mTc-MIBI SPECT: A Meta-Analysis. *Acta Radiol.* **2016**, *58*, 558–564. [[CrossRef](#)]
68. Lenschow, C.; Gassmann, P.; Wenning, C.; Senninger, N.; Colombo-Benkmann, M. Preoperative ¹¹C-Methionine PET/CT Enables Focused Parathyroidectomy in MIBI-SPECT Negative Parathyroid Adenoma. *World J. Surg.* **2015**, *39*, 1750–1757. [[CrossRef](#)]
69. Hotta, M.; Minamimoto, R.; Miwa, K. 11C-Methionine-PET for Differentiating Recurrent Brain Tumor from Radiation Necrosis: Radiomics Approach with Random Forest Classifier. *Sci. Rep.* **2019**, *9*, 15666. [[CrossRef](#)]
70. He, Q.; Zhang, L.; Zhang, B.; Shi, X.; Yi, C.; Zhang, X. Diagnostic Accuracy of 13N-Ammonia PET, 11C-Methionine PET and 18F-Fluorodeoxyglucose PET: A Comparative Study in Patients with Suspected Cerebral Glioma. *BMC Cancer* **2019**, *19*, 332. [[CrossRef](#)]
71. Wedman, J.; Pruim, J.; Putten, L.; Hoekstra, O.S.; Bree, R.; Dijk, B.A.C.; Laan, B.F.A.M. Is C-11 Methionine PET an Alternative to 18-F FDG-PET for Identifying Recurrent Laryngeal Cancer after Radiotherapy? *Clin. Otolaryngol.* **2019**, *44*, 124–130. [[CrossRef](#)]
72. Phan, H.T.T.; Jager, P.L.; Plukker, J.T.M.; Wolffenbuttel, B.H.R.; Dierckx, R.A.; Links, T.P. Comparison of 11C-Methionine PET and 18F-Fluorodeoxyglucose PET in Differentiated Thyroid Cancer. *Nucl. Med. Commun.* **2008**, *29*, 711–716. [[CrossRef](#)] [[PubMed](#)]
73. Morimoto, M.; Kudomi, N.; Maeda, Y.; Kobata, T.; Oishi, A.; Matsumoto, K.; Monden, T.; Iwasaki, T.; Mitamura, K.; Norikane, T.; et al. Effect of Quantitative Values on Shortened Acquisition Duration in Brain Tumor 11C-Methionine PET/CT. *EJNMMI Phys.* **2021**, *8*, 34. [[CrossRef](#)] [[PubMed](#)]
74. Nguyen, T.-L.; Durán, R.V. Glutamine Metabolism in Cancer Therapy. *Cancer Drug Resist.* **2018**. [[CrossRef](#)]
75. Sohda, M.; Miyazaki, T.; Honjyo, H.; Hara, K.; Ozawa, D.; Sakai, M.; Yokobori, T.; Higuchi, T.; Tsushima, Y.; Kuwano, H. 18F-FAMT PET Is Useful to Distinguish between Specific Uptake and Nonspecific Uptake Compared to 18F-Fluorodeoxyglucose Position Emission Tomography in Esophageal Cancer Patients. *Dig. Surg.* **2018**, *35*, 383–388. [[CrossRef](#)]
76. Wei, L.; Tominaga, H.; Ohgaki, R.; Wiriyasermkul, P.; Hagiwara, K.; Okuda, S.; Kaira, K.; Oriuchi, N.; Nagamori, S.; Kanai, Y. Specific Transport of 3-fluoro-l- α -methyl-tyrosine by LAT1 Explains Its Specificity to Malignant Tumors in Imaging. *Cancer Sci.* **2016**, *107*, 347–352. [[CrossRef](#)]
77. Wiriyasermkul, P.; Nagamori, S.; Tominaga, H.; Oriuchi, N.; Kaira, K.; Nakao, H.; Kitashoji, T.; Ohgaki, R.; Tanaka, H.; Endou, H.; et al. Transport of 3-Fluoro-l- α -Methyl-Tyrosine by Tumor-Upregulated L-Type Amino Acid Transporter 1: A Cause of the Tumor Uptake in PET. *J. Nucl. Med.* **2012**, *53*, 1253–1261. [[CrossRef](#)]
78. Saidijam, M.; Afshar, S.; Ahmad, I.; Patching, S. Nucleoside Transporters in PET Imaging of Proliferating Cancer Cells Using 3'-Deoxy-3'-[18F]Fluoro-L-Thymidine. *J. Diagn. Imaging* **2018**, *5*, 1–13. [[CrossRef](#)]
79. Nakajo, M.; Nakajo, M.; Jinguji, M.; Tani, A.; Kajiya, Y.; Tanabe, H.; Fukukura, Y.; Nakabeppu, Y.; Koriyama, C. Diagnosis of Metastases from Postoperative Differentiated Thyroid Cancer: Comparison between FDG and FLT PET/CT Studies. *Radiology* **2013**, *267*, 891–901. [[CrossRef](#)]
80. Sun, X.; Li, Y.; Liu, T.; Li, Z.; Zhang, X.; Chen, X. Peptide-Based Imaging Agents for Cancer Detection. *Adv. Drug Deliv. Rev.* **2017**, *110*, 38–51. [[CrossRef](#)]
81. Pauwels, E.; Cleeren, F.; Bormans, G.; Deroose, C.M. Somatostatin Receptor PET Ligands-the next Generation for Clinical Practice. *Am. J. Nucl. Med. Mol. Imaging* **2018**, *8*, 311–331.
82. Staderini, M.; Megia-Fernandez, A.; Dhaliwal, K.; Bradley, M. Peptides for Optical Medical Imaging and Steps towards Therapy. *Bioorg. Med. Chem.* **2018**, *26*, 2816–2826. [[CrossRef](#)]
83. Treglia, G.; Tamburello, A.; Giovanella, L. Detection Rate of Somatostatin Receptor PET in Patients with Recurrent Medullary Thyroid Carcinoma: A Systematic Review and a Meta-Analysis. *Horm. Athens Greece* **2017**, *16*, 262–272. [[CrossRef](#)]
84. Agthoven, J.F.V.; Xiong, J.-P.; Alonso, J.L.; Rui, X.; Adair, B.D.; Goodman, S.L.; Arnaout, M.A. Structural Basis for Pure Antagonism of Integrin AV β 3 by a High-Affinity Form of Fibronectin. *Nat. Struct. Mol. Biol.* **2014**, *21*, 383–388. [[CrossRef](#)]

85. Parihar, A.S.; Mittal, B.R.; Kumar, R.; Shukla, J.; Bhattacharya, A. ⁶⁸Ga-DOTA-RGD2 Positron Emission Tomography/Computed Tomography in Radioiodine Refractory Thyroid Cancer: Prospective Comparison of Diagnostic Accuracy with ¹⁸F-FDG Positron Emission Tomography/Computed Tomography and Evaluation Toward Potential Theranostics. *Thyroid Off. J. Am. Thyroid Assoc.* **2020**, *30*, 557–567. [[CrossRef](#)]
86. Parihar, A.S.; Sood, A.; Kumar, R.; Bhusari, P.; Shukla, J.; Mittal, B.R. Novel Use of ¹⁷⁷Lu-DOTA-RGD2 in Treatment of ⁶⁸Ga-DOTA-RGD2-Avid Lesions in Papillary Thyroid Cancer with TENIS. *Eur. J. Nucl. Med. Mol. Imaging* **2018**, *45*, 1836–1837. [[CrossRef](#)]
87. Heitkötter, B.; Steinestel, K.; Trautmann, M.; Grünwald, I.; Barth, P.; Gevensleben, H.; Bögemann, M.; Wardelmann, E.; Hartmann, W.; Rahbar, K.; et al. Neovascular PSMA Expression Is a Common Feature in Malignant Neoplasms of the Thyroid. *Oncotarget* **2018**, *9*, 9867–9874. [[CrossRef](#)]
88. Sager, S.; Vatankulu, B.; Uslu, L.; Sönmezoglu, K. Incidental Detection of Follicular Thyroid Carcinoma in ⁶⁸Ga-PSMA PET/CT Imaging. *J. Nucl. Med. Technol.* **2016**, *44*, 199–200. [[CrossRef](#)]
89. Bychkov, A.; Vutrapongwatana, U.; Tepmongkol, S.; Keelawat, S. PSMA Expression by Microvasculature of Thyroid Tumors—Potential Implications for PSMA Theranostics. *Sci. Rep.* **2017**, *7*, 5202. [[CrossRef](#)]
90. Taywade, S.K.; Damle, N.A.; Bal, C. PSMA Expression in Papillary Thyroid Carcinoma. *Clin. Nucl. Med.* **2016**, *41*, e263–e265. [[CrossRef](#)]
91. Derlin, T.; Kreipe, H.-H.; Schumacher, U.; Soudah, B. PSMA Expression in Tumor Neovasculature Endothelial Cells of Follicular Thyroid Adenoma as Identified by Molecular Imaging Using ⁶⁸Ga-PSMA Ligand PET/CT. *Clin. Nucl. Med.* **2017**, *42*, e173–e174. [[CrossRef](#)]
92. Khreish, F.; Ebert, N.; Ries, M.; Maus, S.; Rosar, F.; Bohnenberger, H.; Stemler, T.; Saar, M.; Bartholom?, M.; Ezziddin, S. 225 Ac-PSMA-617/ ¹⁷⁷ Lu-PSMA-617 Tandem Therapy of Metastatic Castration-Resistant Prostate Cancer: Pilot Experience. *Nuklearmed* **2020**, *59*, 93. [[CrossRef](#)]
93. Klingler, M.; Rangger, C.; Summer, D.; Kaeopookum, P.; Decristoforo, C.; Guggenberg, E. von Cholecystokinin-2 Receptor Targeting with Novel C-Terminally Stabilized HYNIC-Minigastrin Analogs Radiolabeled with Technetium-99m. *Pharm* **2019**, *12*, 13. [[CrossRef](#)]
94. Klingler, M.; Hörmann, A.A.; Guggenberg, E.V. Cholecystokinin-2 Receptor Targeting with Radiolabeled Peptides: Current Status and Future Directions. *Curr. Med. Chem.* **2020**, *27*, 7112–7132. [[CrossRef](#)] [[PubMed](#)]
95. Klingler, M.; Summer, D.; Rangger, C.; Haubner, R.; Foster, J.; Sosabowski, J.; Decristoforo, C.; Virgolini, I.; Guggenberg, E. von DOTA-MGS5, a New Cholecystokinin-2 Receptor-Targeting Peptide Analog with an Optimized Targeting Profile for Theranostic Use. *J. Nucl. Med.* **2018**, *60*, 1010–1016. [[CrossRef](#)] [[PubMed](#)]
96. Uprimny, C.; von Guggenberg, E.; Svirydenka, A.; Mikołajczak, R.; Hubalewska-Dydejczyk, A.; Virgolini, I.J. Comparison of PET/CT Imaging with [¹⁸F]FDOPA and Cholecystokinin-2 Receptor Targeting [⁶⁸Ga]Ga-DOTA-MGS5 in a Patient with Advanced Medullary Thyroid Carcinoma. *Eur. J. Nucl. Med. Mol. Imaging* **2020**, 1–2. [[CrossRef](#)]
97. Zahavi, D.; Weiner, L. Monoclonal Antibodies in Cancer Therapy. *Antibodies* **2020**, *9*, 34. [[CrossRef](#)]
98. Lu, R.-M.; Hwang, Y.-C.; Liu, I.-J.; Lee, C.-C.; Tsai, H.-Z.; Li, H.-J.; Wu, H.-C. Development of Therapeutic Antibodies for the Treatment of Diseases. *J. Biomed. Sci.* **2020**, *27*, 1. [[CrossRef](#)]
99. Keizer, R.J.; Huitema, A.D.R.; Schellens, J.H.M.; Beijnen, J.H. Clinical Pharmacokinetics of Therapeutic Monoclonal Antibodies. *Clin. Pharm.* **2010**, *49*, 493–507. [[CrossRef](#)]
100. Warram, J.M.; de Boer, E.; Sorace, A.G.; Chung, T.K.; Kim, H.; Pleijhuis, R.G.; van Dam, G.M.; Rosenthal, E.L. Antibody-Based Imaging Strategies for Cancer. *Cancer Metastasis Rev.* **2014**, *33*, 809–822. [[CrossRef](#)]
101. Wei, W.; Jiang, D.; Lee, H.J.; Li, M.; Kuttyreff, C.J.; Engle, J.W.; Liu, J.; Cai, W. Development and Characterization of CD54-Targeted ImmunoPET Imaging in Solid Tumors. *Eur. J. Nucl. Med. Mol. Imaging* **2020**, *47*, 2765–2775. [[CrossRef](#)]
102. Iqbal, N.; Iqbal, N. Human Epidermal Growth Factor Receptor 2 (HER2) in Cancers: Overexpression and Therapeutic Implications. *Mol. Biol. Int.* **2014**, *2014*, 852748. [[CrossRef](#)]
103. Jiang, D.; Im, H.-J.; Sun, H.; Valdovinos, H.F.; England, C.G.; Ehlerding, E.B.; Nickles, R.J.; Lee, D.S.; Cho, S.Y.; Huang, P.; et al. Radiolabeled Pertuzumab for Imaging of Human Epidermal Growth Factor Receptor 2 Expression in Ovarian Cancer. *Eur. J. Nucl. Med. Mol. Imaging* **2017**, *44*, 1296–1305. [[CrossRef](#)]
104. Hyman, D.M.; Piha-Paul, S.A.; Won, H.; Rodon, J.; Saura, C.; Shapiro, G.I.; Juric, D.; Quinn, D.I.; Moreno, V.; Doger, B.; et al. HER Kinase Inhibition in Patients with HER2- and HER3-Mutant Cancers. *Nature* **2018**, *554*, 189–194. [[CrossRef](#)]
105. Ruggeri, R.M.; Campenni, A.; Giuffrè, G.; Giovanella, L.; Siracusa, M.; Simone, A.; Branca, G.; Scarfi, R.; Trimarchi, F.; Ieni, A.; et al. HER2 Analysis in Sporadic Thyroid Cancer of Follicular Cell Origin. *Int. J. Mol. Sci.* **2016**, *17*, 2040. [[CrossRef](#)]
106. Kunstman, J.W.; Juhlin, C.C.; Goh, G.; Brown, T.C.; Stenman, A.; Healy, J.M.; Rubinstein, J.C.; Choi, M.; Kiss, N.; Nelson-Williams, C.; et al. Characterization of the Mutational Landscape of Anaplastic Thyroid Cancer via Whole-Exome Sequencing. *Hum. Mol. Genet.* **2015**, *24*, 2318–2329. [[CrossRef](#)]
107. Ahmed, S.; Sami, A.; Xiang, J. HER2-Directed Therapy: Current Treatment Options for HER2-Positive Breast Cancer. *Breast Cancer* **2015**, *22*, 101–116. [[CrossRef](#)]
108. Pondé, N.F.; Zardavas, D.; Piccart, M. Progress in Adjuvant Systemic Therapy for Breast Cancer. *Nat. Rev. Clin. Oncol.* **2019**, *16*, 27–44. [[CrossRef](#)]

109. Bardhan, P.; Bui, M.M.; Minton, S.; Loftus, L.; Carter, W.B.; Laronga, C.; Ismail-Khan, R. HER2-Positive Male Breast Cancer with Thyroid Cancer: An Institutional Report and Review of Literature. *Ann. Clin. Lab. Sci.* **2012**, *42*, 135–139.
110. Handkiewicz-Junak, D.; Swierniak, M.; Rusinek, D.; Oczko-Wojciechowska, M.; Dom, G.; Maenhaut, C.; Unger, K.; Detours, V.; Bogdanova, T.; Thomas, G.; et al. Gene Signature of the Post-Chernobyl Papillary Thyroid Cancer. *Eur. J. Nucl. Med. Mol. Imaging* **2016**, *43*, 1267–1277. [[CrossRef](#)]
111. Yan, M.; Schwaederle, M.; Arguello, D.; Millis, S.Z.; Gatalica, Z.; Kurzrock, R. HER2 Expression Status in Diverse Cancers: Review of Results from 37,992 Patients. *Cancer Metastasis Rev.* **2015**, *34*, 157–164. [[CrossRef](#)]
112. Zhang, L.; Zhang, Y.; Mehta, A.; Boufraqueh, M.; Davis, S.; Wang, J.; Tian, Z.; Yu, Z.; Boxer, M.B.; Kiefer, J.A.; et al. Dual Inhibition of HDAC and EGFR Signaling with CUDC-101 Induces Potent Suppression of Tumor Growth and Metastasis in Anaplastic Thyroid Cancer. *Oncotarget* **2015**, *6*, 9073–9085. [[CrossRef](#)]
113. Montero-Conde, C.; Ruiz-Llorente, S.; Dominguez, J.M.; Knauf, J.A.; Viale, A.; Sherman, E.J.; Ryder, M.; Ghossein, R.A.; Rosen, N.; Fagin, J.A. Relief of Feedback Inhibition of HER3 Transcription by RAF and MEK Inhibitors Attenuates Their Antitumor Effects in BRAF-Mutant Thyroid Carcinomas. *Cancer Discov.* **2013**, *3*, 520–533. [[CrossRef](#)]
114. Wei, W.; Jiang, D.; Rosenkrans, Z.T.; Barnhart, T.E.; Engle, J.W.; Luo, Q.; Cai, W. HER2-Targeted Multimodal Imaging of Anaplastic Thyroid Cancer. *Am. J. Cancer Res.* **2019**, *9*, 2413–2427.
115. Reina, M.; Espel, E. Role of LFA-1 and ICAM-1 in Cancer. *Cancers* **2017**, *9*, 153. [[CrossRef](#)]
116. Zhang, P.; Goodrich, C.; Fu, C.; Dong, C. Melanoma Upregulates ICAM-1 Expression on Endothelial Cells through Engagement of Tumor CD44 with Endothelial E-selectin and Activation of a PKC α -P38-SP-1 Pathway. *FASEB J.* **2014**, *28*, 4591–4609. [[CrossRef](#)] [[PubMed](#)]
117. Buitrago, D.; Keutgen, X.M.; Crowley, M.; Filicori, F.; Aldailami, H.; Hoda, R.; Liu, Y.-F.; Hoda, R.S.; Scognamiglio, T.; Jin, M.; et al. Intercellular Adhesion Molecule-1 (ICAM-1) Is Upregulated in Aggressive Papillary Thyroid Carcinoma. *Ann. Surg. Oncol.* **2012**, *19*, 973–980. [[CrossRef](#)] [[PubMed](#)]
118. Galore-Haskel, G.; Baruch, E.N.; Berg, A.L.; Barshack, I.; Zilinsky, I.; Avivi, C.; Besser, M.J.; Schachter, J.; Markel, G. Histopathological Expression Analysis of Intercellular Adhesion Molecule 1 (ICAM-1) along Development and Progression of Human Melanoma. *Oncotarget* **2014**, *5*, 99580–99586. [[CrossRef](#)] [[PubMed](#)]
119. Min, I.M.; Shevlin, E.; Vedvyas, Y.; Zaman, M.; Wyrwas, B.; Scognamiglio, T.; Moore, M.D.; Wang, W.; Park, S.; Park, S.; et al. CAR T Therapy Targeting ICAM-1 Eliminates Advanced Human Thyroid Tumors. *Clin. Cancer Res. Off. J. Am. Assoc. Cancer Res.* **2017**, *23*, 7569–7583. [[CrossRef](#)]
120. Vedvyas, Y.; McCloskey, J.E.; Yang, Y.; Min, I.M.; Fahey, T.J.; Zarnegar, R.; Hsu, Y.-M.S.; Hsu, J.-M.; Besien, K.V.; Gaudet, I.; et al. Manufacturing and Preclinical Validation of CAR T Cells Targeting ICAM-1 for Advanced Thyroid Cancer Therapy. *Sci. Rep.* **2019**, *9*, 10634. [[CrossRef](#)]
121. Li, J.; Vasilyeva, E.; Wiseman, S.M. Beyond Immunohistochemistry and Immunocytochemistry: A Current Perspective on Galectin-3 and Thyroid Cancer. *Expert Rev. Anticancer* **2019**, *19*, 1017–1027. [[CrossRef](#)]
122. Bartolazzi, A.; Gasbarri, A.; Papotti, M.; Bussolati, G.; Lucante, T.; Khan, A.; Inohara, H.; Marandino, F.; Orlandi, F.; Nardi, F.; et al. Application of an Immunodiagnostic Method for Improving Preoperative Diagnosis of Nodular Thyroid Lesions. *Lancet* **2001**, *357*, 1644–1650. [[CrossRef](#)]
123. Bartolazzi, A.; Orlandi, F.; Saggiorato, E.; Volante, M.; Arecco, F.; Rossetto, R.; Palestini, N.; Ghigo, E.; Papotti, M.; Bussolati, G.; et al. Galectin-3-Expression Analysis in the Surgical Selection of Follicular Thyroid Nodules with Indeterminate Fine-Needle Aspiration Cytology: A Prospective Multicentre Study. *Lancet Oncol.* **2008**, *9*, 543–549. [[CrossRef](#)]
124. D'Alessandria, C.; Braesch-Andersen, S.; Bejo, K.; Reder, S.; Blechert, B.; Schwaiger, M.; Bartolazzi, A. Noninvasive In Vivo Imaging and Biologic Characterization of Thyroid Tumors by ImmunoPET Targeting of Galectin-3. *Cancer Res.* **2016**, *76*, 3583–3592. [[CrossRef](#)]
125. Rose, F.D.; Braeuer, M.; Braesch-Andersen, S.; Otto, A.M.; Steiger, K.; Reder, S.; Mall, S.; Nekolla, S.; Schwaiger, M.; Weber, W.A.; et al. Galectin-3 Targeting in Thyroid Orthotopic Tumors Opens New Ways to Characterize Thyroid Cancer. *J. Nucl. Med.* **2019**, *60*, 770–776. [[CrossRef](#)]
126. Nair, L.M.; Anila, K.R.; Sreekumar, A.; Pradeep, V.M. Renal Metastasis from Papillary Carcinoma Thyroid Detected by Whole Body Iodine Scan: A Case Report and Review of the Literature. *Indian J. Nucl. Med. IJNM Off. J. Soc. Nucl. Med. India* **2016**, *31*, 232–234. [[CrossRef](#)]
127. Fan, G.; Wang, Z.; Hao, M.; Li, J. Bispecific Antibodies and Their Applications. *J. Hematol. Oncol.* **2015**, *8*, 130. [[CrossRef](#)]
128. Krishnamurthy, A.; Jimeno, A. Bispecific Antibodies for Cancer Therapy: A Review. *Pharm. Ther.* **2017**, *185*, 122–134. [[CrossRef](#)]
129. Oudoux, A.; Salaun, P.-Y.; Bournaud, C.; Campion, L.; Ansquer, C.; Rousseau, C.; Bardet, S.; Borson-Chazot, F.; Vuillez, J.-P.; Murat, A.; et al. Sensitivity and Prognostic Value of Positron Emission Tomography with F-18-Fluorodeoxyglucose and Sensitivity of Immunoscintigraphy in Patients with Medullary Thyroid Carcinoma Treated with Anticarcinoembryonic Antigen-Targeted Radioimmunotherapy. *J. Clin. Endocrinol. Metab.* **2007**, *92*, 4590–4597. [[CrossRef](#)]
130. Peltier, P.; Curtet, C.; Chatal, J.F.; Doussal, J.M.L.; Daniel, G.; Aillet, G.; Gruaz-Guyon, A.; Barbet, J.; Delaage, M. Radioimmunodetection of Medullary Thyroid Cancer Using a Bispecific Anti-CEA / Anti-Indium-DTPA Antibody and an Indium-111-Labeled DTPA Dimer. *J. Nucl. Med. Off. Publ. Soc. Nucl. Med.* **1993**, *34*, 1267–1273.
131. Barbet, J.; Peltier, P.; Bardet, S.; Vuillez, J.P.; Bachelot, I.; Denet, S.; Olivier, P.; Leccia, F.; Corcuff, B.; Huglo, D.; et al. Radiotheranostics: A Roadmap for Future Development. *Lancet Oncol.* **2020**, *21*, e146–e156. [[CrossRef](#)]

132. Kraeber-Bodéré, F.; Salaun, P.-Y.; Ansquer, C.; Drui, D.; Mirallié, E.; Faivre-Chauvet, A.; Barbet, J.; Goldenberg, D.M.; Chatal, J.-F. Pretargeted Radioimmunotherapy (PRAIT) in Medullary Thyroid Cancer (MTC). *Tumor Biol.* **2012**, *33*, 601–606. [[CrossRef](#)]
133. Schoffelen, R.; Boerman, O.C.; Goldenberg, D.M.; Sharkey, R.M.; van Herpen, C.M.L.; Franssen, G.M.; McBride, W.J.; Chang, C.-H.; Rossi, E.A.; van der Graaf, W.T.A.; et al. Development of an Imaging-Guided CEA-Pretargeted Radionuclide Treatment of Advanced Colorectal Cancer: First Clinical Results. *Brit. J. Cancer* **2013**, *109*, 934–942. [[CrossRef](#)]
134. Bodet-Milin, C.; Faivre-Chauvet, A.; Carlier, T.; Rauscher, A.; Bourgeois, M.; Cerato, E.; Rohmer, V.; Couturier, O.; Drui, D.; Goldenberg, D.M.; et al. Immuno-PET Using Anticarcinoembryonic Antigen Bispecific Antibody and ⁶⁸Ga-Labeled Peptide in Metastatic Medullary Thyroid Carcinoma: Clinical Optimization of the Pretargeting Parameters in a First-in-Human Trial. *J. Nucl. Med.* **2016**, *57*, 1505–1511. [[CrossRef](#)]
135. Bates, A.; Power, C.A. David vs. Goliath: The Structure, Function, and Clinical Prospects of Antibody Fragments. *Antibodies* **2019**, *8*, 28. [[CrossRef](#)]
136. Kulmala, A.; Huovinen, T.; Lamminmäki, U. Improvement of Fab Expression by Screening Combinatorial Synonymous Signal Sequence Libraries. *Microb. Cell Factories* **2019**, *18*, 157. [[CrossRef](#)]
137. Xenaki, K.T.; Oliveira, S.; van Bergen En Henegouwen, P.M.P. Antibody or Antibody Fragments: Implications for Molecular Imaging and Targeted Therapy of Solid Tumors. *Front. Immunol.* **2017**, *8*, 1287. [[CrossRef](#)]
138. Duan, H.; Huang, H.; Jing, G. An Antibody Fab Fragment-Based Chimeric Antigen Receptor Could Efficiently Eliminate Human Thyroid Cancer Cells. *J. Cancer* **2019**, *10*, 1890–1895. [[CrossRef](#)]
139. Peplau, E.; Rose, F.D.; Reder, S.; Mittelhäuser, M.; Scafetta, G.; Schwaiger, M.; Weber, W.A.; Bartolazzi, A.; Skerra, A.; D'Alessandria, C. Development of a Chimeric Antigen-Binding Fragment Directed Against Human Galectin-3 and Validation as an Immuno-Positron Emission Tomography Tracer for the Sensitive In Vivo Imaging of Thyroid Cancer. *Thyroid* **2020**, *30*, 1314–1326. [[CrossRef](#)]
140. Peplau, E.; Rose, F.D.; Eichinger, A.; Reder, S.; Mittelhäuser, M.; Scafetta, G.; Schwaiger, M.; Weber, W.A.; Bartolazzi, A.; D'Alessandria, C.; et al. Effective Rational Humanization of a PASylated Anti-Galectin-3 Fab for the Sensitive PET Imaging of Thyroid Cancer in Vivo. *Sci. Rep.* **2021**, *11*, 7358. [[CrossRef](#)]
141. Wu, Y.; Jiang, S.; Ying, T. Single-Domain Antibodies as Therapeutics against Human Viral Diseases. *Front. Immunol.* **2017**, *8*, 1802. [[CrossRef](#)] [[PubMed](#)]
142. Pleiner, T.; Bates, M.; Trakhanov, S.; Lee, C.-T.; Schliep, J.E.; Chug, H.; Böhning, M.; Stark, H.; Urlaub, H.; Görlich, D. Nanobodies: Site-Specific Labeling for Super-Resolution Imaging, Rapid Epitope-Mapping and Native Protein Complex Isolation. *Elife* **2015**, *4*, e11349. [[CrossRef](#)] [[PubMed](#)]
143. Jaikhani, N.; Ingram, J.R.; Rashidian, M.; Rickelt, S.; Tian, C.; Mak, H.; Jiang, Z.; Ploegh, H.L.; Hynes, R.O. Noninvasive Imaging of Tumor Progression, Metastasis, and Fibrosis Using a Nanobody Targeting the Extracellular Matrix. *Proc. Natl. Acad. Sci. USA* **2019**, *116*, 14181–14190. [[CrossRef](#)] [[PubMed](#)]
144. Li, J.; Zhou, C.; Dong, B.; Zhong, H.; Chen, S.; Li, Q.; Wang, Z. Single Domain Antibody-Based Bispecific Antibody Induces Potent Specific Anti-Tumor Activity. *Cancer Biol.* **2016**, *17*, 1231–1239. [[CrossRef](#)] [[PubMed](#)]
145. Guo, W.; Zhang, C.; Ma, T.; Liu, X.; Chen, Z.; Li, S.; Deng, Y. Advances in Aptamer Screening and Aptasensors' Detection of Heavy Metal Ions. *J. Nanobiotechnol.* **2021**, *19*, 166. [[CrossRef](#)]
146. Zhou, J.; Rossi, J. Aptamers as Targeted Therapeutics: Current Potential and Challenges. *Nat. Rev. Drug Discov.* **2016**, *16*, 181–202. [[CrossRef](#)]
147. Behrooz, A.B.; Syahir, A.; Ahmad, S. CD133: Beyond a Cancer Stem Cell Biomarker. *J. Drug Target.* **2018**, *27*, 1–31. [[CrossRef](#)]
148. Yang, Z.-L.; Zheng, Q.; Yan, J.; Pan, Y.; Wang, Z.-G. Upregulated CD133 Expression in Tumorigenesis of Colon Cancer Cells. *World J. Gastroenterol.* **2011**, *17*, 932–937. [[CrossRef](#)]
149. Dhaybi, R.A.; Sartelet, H.; Powell, J.; Kokta, V. Expression of CD133+ Cancer Stem Cells in Childhood Malignant Melanoma and Its Correlation with Metastasis. *Mod. Pathol.* **2010**, *23*, 376–380. [[CrossRef](#)]
150. Liu, J.; Brown, R.E. Immunohistochemical Detection of Epithelial-mesenchymal Transition Associated with Stemness Phenotype in Anaplastic Thyroid Carcinoma. *Int. J. Clin. Exp. Pathol.* **2010**, *3*, 755–762.
151. Glumac, P.M.; LeBeau, A.M. The Role of CD133 in Cancer: A Concise Review. *Clin. Transl. Med.* **2018**, *7*, 18. [[CrossRef](#)]
152. Friedman, S.; Lu, M.; Schultz, A.; Thomas, D.; Lin, R.-Y. CD133+ Anaplastic Thyroid Cancer Cells Initiate Tumors in Immunodeficient Mice and Are Regulated by Thyrotropin. *PLoS ONE* **2009**, *4*, e5395. [[CrossRef](#)]
153. Lin, Z.; Lu, X.; Li, W.; Sun, M.; Peng, M.; Yang, H.; Chen, L.; Zhang, C.; Cai, L.; Li, Y. Association of Cancer Stem Cell Markers with Aggressive Tumor Features in Papillary Thyroid Carcinoma. *Cancer Control.* **2015**, *22*, 508–514. [[CrossRef](#)]
154. Wang, Y.; Sui, G.; Teng, D.; Wang, Q.; Qu, J.; Zhu, L.; Ran, H.; Wang, Z.; Jin, C.; Wang, H. Low Intensity Focused Ultrasound (LIFU) Triggered Drug Release from Cetuximab-Conjugated Phase-Changeable Nanoparticles for Precision Theranostics against Anaplastic Thyroid Carcinoma. *Biomater. Sci.* **2018**, *7*, 196–210. [[CrossRef](#)]
155. Hu, Z.; Qin, J.; Li, T.; Guo, J. Thyroid Cancer MR Molecular Imaging via SHP2-Targeted Nanoparticles. *Int. J. Nanomed.* **2019**, *14*, 7365–7373. [[CrossRef](#)]
156. Ayati, A.; Moghimi, S.; Toolabi, M.; Foroumadi, A. Pyrimidine-Based EGFR TK Inhibitors in Targeted Cancer Therapy. *Eur. J. Med. Chem.* **2021**, *221*, 113523. [[CrossRef](#)]
157. Hu, Z.-Q.; Ma, R.; Zhang, C.-M.; Li, J.; Li, L.; Hu, Z.-T.; Gao, Q.; Li, W.-M. Expression and Clinical Significance of Tyrosine Phosphatase SHP2 in Thyroid Carcinoma. *Oncol. Lett.* **2015**, *10*, 1507–1512. [[CrossRef](#)]

158. Wei, W.-J.; Hardin, H.; Luo, Q.-Y. Targeting Autophagy in Thyroid Cancers. *Endocr. Relat. Cancer* **2019**, *1*, R181–R194. [[CrossRef](#)]
159. Jin, Y.; Liu, M.; Sa, R.; Fu, H.; Cheng, L.; Chen, L. Mouse Models of Thyroid Cancer: Bridging Pathogenesis and Novel Therapeutics. *Cancer Lett* **2020**, *469*, 35–53. [[CrossRef](#)]
160. Nakajo, M.; Nakajo, M.; Kajiya, Y.; Jinguji, M.; Mori, S.; Aridome, K.; Suenaga, T.; Tanaka, S. High FDG and Low FLT Uptake in a Thyroid Papillary Carcinoma Incidentally Discovered by FDG PET/CT. *Clin. Nucl. Med.* **2012**, *37*, 607. [[CrossRef](#)]
161. Souteiro, P.; Gouveia, P.; Ferreira, G.; Belo, S.; Costa, C.; Carvalho, D.; Duarte, H.; Sampaio, I.L. ⁶⁸Ga-DOTANOC and ¹⁸F-FDG PET/CT in Metastatic Medullary Thyroid Carcinoma: Novel Correlations with Tumoral Biomarkers. *Endocrine* **2019**, *64*, 322–329. [[CrossRef](#)]
162. Budiawan, H.; Salavati, A.; Kulkarni, H.R.; Baum, R.P. Peptide Receptor Radionuclide Therapy of Treatment-Refractory Metastatic Thyroid Cancer Using (⁹⁰Yttrium and (¹⁷⁷Lutetium Labeled Somatostatin Analogs: Toxicity, Response and Survival Analysis. *Am. J. Nucl. Med. Mol. Imaging* **2013**, *4*, 39–52. [[CrossRef](#)]
163. Salavati, A.; Puranik, A.; Kulkarni, H.R.; Budiawan, H.; Baum, R.P. Peptide Receptor Radionuclide Therapy (PRRT) of Medullary and Nonmedullary Thyroid Cancer Using Radiolabeled Somatostatin Analogues. *Semin. Nucl. Med.* **2016**, *46*, 215–224. [[CrossRef](#)]
164. Assadi, M.; Ahmadzadehfar, H. ¹⁷⁷Lu-DOTATATE and ¹⁷⁷Lu-Prostate-Specific Membrane Antigen Therapy in a Patient with Advanced Metastatic Radioiodine-Refractory Differentiated Thyroid Cancer after Failure of Tyrosine Kinase Inhibitors Treatment. *World J. Nucl. Med.* **2019**, *18*, 406. [[CrossRef](#)]
165. De Vries, L.H.; Lodewijk, L.; Braat, A.J.A.T.; Krijger, G.C.; Valk, G.D.; Lam, M.G.E.H.; Rinkes, I.H.M.B.; Vriens, M.R.; Keizer, B. de ⁶⁸Ga-PSMA PET/CT in Radioactive Iodine-Refractory Differentiated Thyroid Cancer and First Treatment Results with ¹⁷⁷Lu-PSMA-617. *EJNMMI Res.* **2020**, *10*, 18. [[CrossRef](#)]
166. Bodet-Milin, C.; Bailly, C.; Toucheffeu, Y.; Frampas, E.; Bourgeois, M.; Rauscher, A.; Lacoëuille, F.; Drui, D.; Arlicot, N.; Goldenberg, D.M.; et al. Clinical Results in Medullary Thyroid Carcinoma Suggest High Potential of Pretargeted Immuno-PET for Tumor Imaging and Theranostic Approaches. *Front. Med.* **2019**, *6*, 124. [[CrossRef](#)]
167. Liu, H.; Shi, J.; Lin, F. The Potential Diagnostic Utility of TROP-2 in Thyroid Neoplasms. *Appl. Immunohistochem. Mol. Morphol.* **2017**, *25*, 525–533. [[CrossRef](#)] [[PubMed](#)]
168. Schürch, C.M.; Roelli, M.A.; Forster, S.; Wasmer, M.-H.; Brühl, F.; Maire, R.S.; Pancrazio, S.D.; Ruepp, M.-D.; Giger, R.; Perren, A.; et al. Targeting CD47 in Anaplastic Thyroid Carcinoma Enhances Tumor Phagocytosis by Macrophages and Is a Promising Therapeutic Strategy. *Thyroid* **2019**, *29*, 979–992. [[CrossRef](#)] [[PubMed](#)]
169. Elmageed, Z.Y.A.; Moroz, K.; Kandil, E. Clinical Significance of CD146 and Latexin during Different Stages of Thyroid Cancer. *Mol. Cell Biochem.* **2013**, *381*, 95–103. [[CrossRef](#)] [[PubMed](#)]
170. Ehlerding, E.B.; Sun, L.; Lan, X.; Zeng, D.; Cai, W. Dual-Targeted Molecular Imaging of Cancer. *J. Nucl. Med.* **2018**, *59*, 390–395. [[CrossRef](#)] [[PubMed](#)]
171. Morais, M.; Ma, M.T. Site-Specific Chelator-Antibody Conjugation for PET and SPECT Imaging with Radiometals. *Drug Discov. Today Technol.* **2018**, *30*, 91–104. [[CrossRef](#)] [[PubMed](#)]
172. Li, L.; Crow, D.; Turatti, F.; Bading, J.R.; Anderson, A.-L.; Poku, E.; Yazaki, P.J.; Carmichael, J.; Leong, D.; Wheatcroft, D.; et al. Site-Specific Conjugation of Monodispersed DOTA-PEGn to a Thiolated Diabody Reveals the Effect of Increasing PEG Size on Kidney Clearance and Tumor Uptake with Improved ⁶⁴Copper PET Imaging. *Bioconjugate Chem.* **2011**, *22*, 709–716. [[CrossRef](#)]
173. Acchione, M.; Kwon, H.; Jochheim, C.M.; Atkins, W.M. Impact of Linker and Conjugation Chemistry on Antigen Binding, Fc Receptor Binding and Thermal Stability of Model Antibody-Drug Conjugates. *mAbs* **2012**, *4*, 362–372. [[CrossRef](#)]
174. Adumeau, P.; Sharma, S.K.; Brent, C.; Zeglis, B.M. Site-Specifically Labeled Immunoconjugates for Molecular Imaging—Part 1: Cysteine Residues and Glycans. *Mol. Imaging Biol.* **2016**, *18*, 1–17. [[CrossRef](#)]
175. Chen, Z.-Y.; Wang, Y.-X.; Lin, Y.; Zhang, J.-S.; Yang, F.; Zhou, Q.-L.; Liao, Y.-Y. Advance of Molecular Imaging Technology and Targeted Imaging Agent in Imaging and Therapy. *BioMed Res. Int.* **2014**, *2014*, 819324. [[CrossRef](#)]
176. Rosenbaum-Krumme, S.J.; Görges, R.; Bockisch, A.; Binse, I. ¹⁸F-FDG PET/CT Changes Therapy Management in High-Risk DTC after First Radioiodine Therapy. *Eur. J. Nucl. Med. Mol. Imaging* **2012**, *39*, 1373–1380. [[CrossRef](#)]
177. Müller, C.; van der Meulen, N.P.; Benešová, M.; Schibli, R. Therapeutic Radiometals Beyond ¹⁷⁷Lu and ⁹⁰Y: Production and Application of Promising α -Particle, β -Particle, and Auger Electron Emitters. *J. Nucl. Med.* **2017**, *58*, 91S–96S. [[CrossRef](#)]